UNIVERSITÀ DEGLI STUDI DI PADOVA

Dipartimento di Fisica e Astronomia "Galileo Galilei"

Corso di Laurea Magistrale in Fisica

Tesi di Laurea

Primordial Black Holes from Inflation

Relatore

Prof. Nicola Bartolo

Correlatori

Dr. Alvise Raccanelli

Prof. Sabino Matarrese

Laureanda

Alba Kalaja

Mat. 1157327

Anno Accademico 2017/2018

Abstract: The study of Primordial Black Holes (PBHs) allows us to gain a deep insight into the early Universe since it gives access to much smaller scales than the CMB scales and it could potentially put strict limits on inflationary models. This thesis aims to put an upper limit on the amplitude of the power spectrum associated to the formation of a PBH by means of recent observational constraints on the PBHs abundance. We use the results of recent numerical simulations in the framework of the general relativistic collapse and peaks theory to connect the formation of PBHs in real space to a generic feature in the primordial curvature power spectrum. Moreover, we investigate the effects that the choice of a particular window function has on the power spectrum.

Contents

Chapter 1

Introduction

One of the most promising research field in modern cosmology is represented by the study of the early Universe. In this context, the theory of inflation plays a major role. Despite the successful confirmations by several observations, the understanding of inflationary mechanism is still far from being complete. In this scenario, the study of primordial black holes (PBHs) could potentially contribute from a theoretical as well as an observational point of view. Such object could have formed during the early universe because of large density fluctuations that collapse gravitationally to form a black hole. As it can be seen in figure 1.1 taken from Ref. [1], the possible existence of PBHs allows the investigation of much smaller scales than those accessed by observation of the Cosmic Microwave Background radiation (CMB) and Large Scale Structure (LSS) among many.

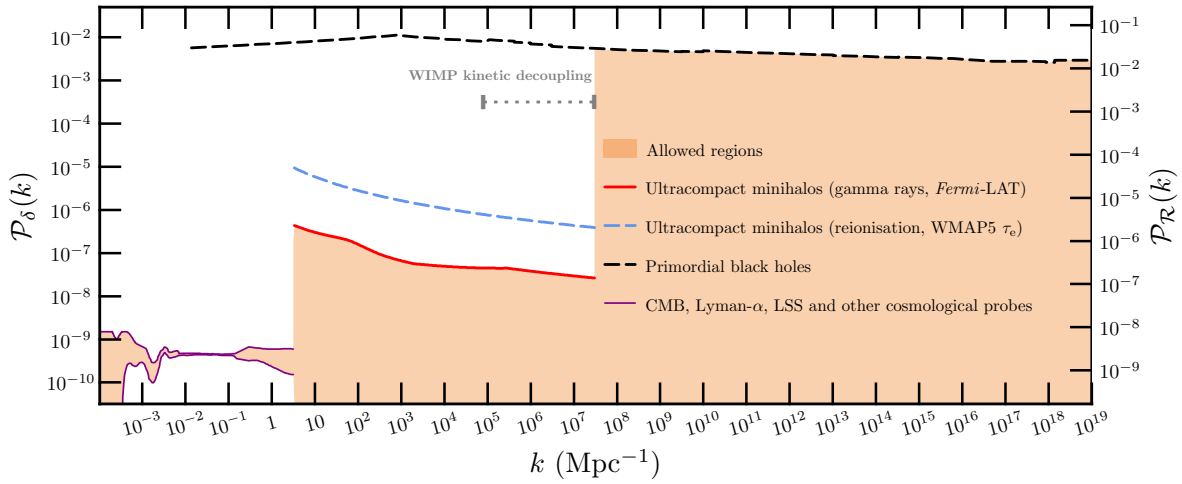

Figure 1.1: Current constraints on the primordial curvature power spectrum.

In addition to this, the recent detection of binary black hole mergers through gravitational waves by the LIGO-Virgo collaboration [9] has brought a significant increase of interest in models where primordial black holes constitute a relevant fraction of dark matter. As a matter of fact, the nature of dark matter is yet to be clarified and PBHs are viable candidates.

In this work we employ the results of recent numerical simulations in the framework of the general relativistic collapse of primordial black holes to connect their formation in real space

to a generic feature in the primordial curvature power spectrum. The main goal is to use the current constraints we have from observations to put an upper limit on the amplitude of the primordial power spectrum.

This work is organised as follows: in chapter 2 we review the inflationary mechanism during which the perturbation that eventually collapse into PBHs are generated; in chapter 3 we summarize the details of PBHs formation; in chapter 4 we explore the main aspect of peaks theory and we apply the results to the theory of PBHs formation; in chapter 5 we explain how to connect perturbations in the geometry of spacetime to perturbations in the radiation field, including a broad discussion on the choice of a window function 5.2, and we present the results of our work.

Notation: In this work we use natural units$c = 1$ and $\hbar = 1$ unless specified. The metric signature used throughout the following discussion is $(-,+,+,+)$. Finally, our Fourier transform convention reads as

$$f(\mathbf{r}) = \int \frac{d^3k}{(2\pi)^3} f(\mathbf{k}) e^{i\mathbf{k}\cdot\mathbf{r}}, \qquad f(\mathbf{k}) = \int d^3r f(\mathbf{r}) e^{-i\mathbf{k}\cdot\mathbf{r}}. \tag{1.1}$$

1.1 The homogeneous and isotropic Universe

In this section, we review the basic aspects of the Hot Big Bang (HBB) theory which are relevant for the following parts of this work (see e.g. Ref. [2, 3, 4, 5]).

The cornerstone of modern cosmology is the cosmological principle, which states that at least on large scales the Universe is homogeneous and isotropic, implying respectively no privileged position nor direction. Despite the fact that at small scales the present Universe is inhomogeneous, with matter clumped into stars, galaxies and clusters of galaxies, the validity of this principle has been confirmed experimentally by the study of the Large Scale Structures (LSS) and the Cosmic Microwave Background (CMB).

The spacetime of the Universe consistent with the cosmological principle is described by the Friedmann-Robertson-Walker (FRW) metric

$$\mathrm{d}s^2 = -c^2\mathrm{d}t^2 + a(t)^2 \left(\frac{\mathrm{d}r^2}{1-kr^2} + r^2\mathrm{d}\theta^2 + r^2\sin^2\theta\mathrm{d}\phi^2 \right), \tag{1.2}$$

where the scale factor $a(t)$ measures the expansion of the Universe and the spatial curvature parameter k can take three values: $k = 0$ in the case of zero curvature and flat Universe, $k = +1$ for positive curvature and closed Universe, $k = -1$ for negative curvature corresponding to a closed Universe. The coordinates used in equation (1.2) refer to an observer comoving with the expansion of the Universe. The physical distance R is given by multiplying the comoving distance r by the scale factor, namely $R = a(t)r$.

Using a coordinate transformation, the metric (1.2) can be recast in

$$\mathrm{d}s^2 = -c^2\mathrm{d}t^2 + a(t)^2 \left[\mathrm{d}\chi^2 + f(\chi)^2(\mathrm{d}\theta^2 + \sin^2\theta\mathrm{d}\phi^2) \right], \tag{1.3}$$

where

$$f(\chi) \equiv \begin{cases} \sinh\chi & k = -1 \\ \chi & k = 0 \\ \sin\chi & k = +1 \end{cases}. \tag{1.4}$$

Another convenient quantity is the conformal time τ defined as

$$\mathrm{d}\tau \equiv \frac{\mathrm{d}t}{a(t)} \quad \Rightarrow \quad \tau \equiv \int \frac{\mathrm{d}t}{a(t)}, \tag{1.5}$$

whereby the FRW metric becomes

$$\mathrm{d}s^2 = a(\tau)^2 \left[-c^2\mathrm{d}\tau^2 + \left(\mathrm{d}\chi^2 + f(\chi)^2(\mathrm{d}\theta^2 + \sin^2\theta \mathrm{d}\phi^2)\right)\right]. \tag{1.6}$$

We see that the metric has factorized into a static Minkowski metric multiplied by a time-dependent conformal factor $a(\tau)$. Hereafter, we distinguish between the derivative with respect to the cosmic time t, denoted with a dot $\dot{}$, and the derivative with respect to the conformal time τ, denoted with a prime $'$.

1.1.1 The Friedmann equations

The dynamics of the Universe is determined by the Hilbert-Einstein and matter actions

$$\mathcal{S}_{HE} + \mathcal{S}_m = \int \mathrm{d}^4\mathrm{x}\sqrt{-g}\left[\frac{R}{16\pi G} + \mathcal{L}_m\right], \tag{1.7}$$

that yields the Einstein equations

$$R_{\mu\nu} - \frac{1}{2}g_{\mu\nu}R = 8\pi G T_{\mu\nu} \tag{1.8}$$

through the principal of least action. Here, $R_{\mu\nu}$ and R are respectively the Ricci tensor and the Ricci scalar. The general definition of stress-energy tensor in the theory of general relativity is

$$T_{\mu\nu} \equiv -\frac{2}{\sqrt{-g}}\frac{\delta\left(\sqrt{-g}\mathcal{L}_m\right)}{\delta g^{\mu\nu}}. \tag{1.9}$$

Assuming that the matter content of the Universe can be described by a perfect fluid, the stress-energy tensor $T_{\mu\nu}$ is given by

$$T_{\mu\nu} = (p + \varrho)u_\mu u_\nu + p g_{\mu\nu}, \tag{1.10}$$

with p the pressure, ϱ the energy density and u_μ the four-velocity of the fluid with $u^\mu u_\mu = -1$. In the fluid rest frame where we may choose $u^\mu = (1, 0, 0, 0)$, therefore the stress-energy tensor is given by

$$T_{\mu\nu} = \begin{bmatrix} \varrho & 0 & 0 & 0 \\ 0 & p & 0 & 0 \\ 0 & 0 & p & 0 \\ 0 & 0 & 0 & p \end{bmatrix}. \tag{1.11}$$

The stress-energy tensor is diagonal and the spatial component of $T_{\mu\nu}$ along the diagonal are all equal since the fluid is perfect.

Applying the FRW metric in equation (1.2) to the Einstein equations, the time-time component yields

$$\frac{\ddot{a}}{a} = -\frac{4\pi G}{3}(\varrho + 3p), \tag{1.12}$$

and the space-space components

$$\frac{\dot{a}^2}{a^2} = H^2 = \frac{8\pi G}{3}\varrho - \frac{k}{a^2}, \tag{1.13}$$

where H is the Hubble parameter. Since the FRW metric is diagonal, the space-time components and the off-diagonal space-space components give $0 = 0$. Finally, from the conservation of stress-energy tensor equation in general relativity

$$D_\mu T^{\mu\nu} = 0, \tag{1.14}$$

where D_μ is the covariant derivative, one obtains the continuity equation

$$\dot{\varrho} = -3\frac{\dot{a}}{a}(\varrho + p). \tag{1.15}$$

To close the system given by equations (1.12), (1.13) and (1.15) we have to specify the equation of state that relates the pressure of the fluid with its energy density. We assume that this is given by

$$p = w\varrho, \tag{1.16}$$

where w is a dimensionless constant. In this case, equation (1.15) yields

$$\frac{d\log\varrho}{d\log a} = -3(1+w) \quad \Rightarrow \quad \varrho \propto a^{-3(1+w)}. \tag{1.17}$$

Combined with the Friedmann equation (1.13), this leads to the time evolution of the scale factor of a flat ($k = 0$) Universe

$$a(t) \propto \begin{cases} t^{\frac{2}{3(1+w)}} & w \neq -1, \\ \mathrm{e}^{Ht} & w = -1, \end{cases} \tag{1.18}$$

or in conformal time

$$a(t) \propto \begin{cases} \tau^{\frac{2}{1+3w}} & w \neq -1, \\ (-\tau)^{-1} & w = -1. \end{cases} \tag{1.19}$$

In particular, for the Universe dominated by non-relativistic matter (dust) $w = 0$, thus $a(t) \propto t^{2/3}$ or equivalently $a(\tau) \propto \tau^2$, whereas the radiation or relativistic matter dominated Universe corresponds to $w = 1/3$, therefore $a(t) \propto t^{1/2}$ and $a(\tau) \propto \tau$. As we shall see next, the second solution in equations (1.18) and (1.19) corresponds to a cosmological constant dominated Universe.

To complete the discussion, we introduce the density parameter Ω, which will become relevant in chapter 2. According to the Einstein equations (1.8), the geometry of the spacetime is intimately related to the distribution of matter-energy. From the Friedmann equation (1.13), one can see that a flat Universe corresponds to a precise value of the energy density given by

$$\varrho_{\mathrm{crit}} = \frac{8\pi G}{3H^2}. \tag{1.20}$$

We define the density parameter $\Omega(t)$ as the ratio between the observed energy density $\varrho(t)$ and the critical one ϱ_{crit}

$$\Omega(t) = \frac{\varrho(t)}{\varrho_{\mathrm{crit}}}, \tag{1.21}$$

which determines the overall geometry of the Universe. In fact, from equation (1.13) we obtain

$$\Omega(t) - 1 = \frac{k}{(aH)^2}. \tag{1.22}$$

Therefore, the space is closed ($k = 1$), flat ($k = 0$) or open ($k = -1$) according to whether the $\Omega(t)$ is greater than, equal to or less than unity.

The details of the evolution of the Universe depends not only on the total energy density ϱ but also on the contributions of the various components present (baryonic matter, photons, etc.). The contribution of the ith component is given by

$$\Omega(t)_{\mathrm{i}} = \frac{\varrho(t)_{\mathrm{i}}}{\varrho_{\mathrm{crit}}}, \tag{1.23}$$

According to the ΛCDM (Cold Dark Matter) model, the contents of the present Universe is divided in Baryonic Matter ($\Omega_{\mathrm{b}} \simeq 0.05$), the ordinary matter made of quarks and leptons; Cold Dark Matter ($\Omega_{\mathrm{cdm}} \simeq 0.26$), the non-luminous matter whose nature is yet to be clarified, the problem is addressed in further details in section 1.2; Radiation ($\Omega_{\mathrm{r}} \simeq 10^{-5}$), that gives a low contribution to the total energy today, but was dominant in the early stages of the Universe, during the so-called radiation dominated era; finally, Dark Energy ($\Omega_\Lambda \simeq 0.68$), a form of energy besides ordinary matter and radiation that could explain the present accelerated expansion of the Universe experimentally observed. In the standard framework, dark energy is described by the cosmological constant (see section 1.1.2), however there is a huge debate concerning the nature of such energy.

1.1.2 The cosmological constant

At the time when Einstein formulated his theory of general relativity, it was generally accepted that the Universe was static. However, a Universe evolving according to the Friedmann equations cannot be static unless $\ddot{a} = 0$, namely

$$\varrho = -3p. \tag{1.24}$$

Since a fluid with such property did not seem to be physically reasonable, Einstein modified equations (1.8) by introducing the cosmological constant term Λ to counterbalance the gravitational attraction

$$R_{\mu\nu} - \frac{1}{2} g_{\mu\nu} R = 8\pi G T_{\mu\nu} - \Lambda g_{\mu\nu}, \tag{1.25}$$

in such a way that it does not change the covariant character of the equations. It can be shown that for an appropriate choice of Λ, one indeed obtains a static cosmological model.

In order to recover a form similar to the equations (1.8), we rewrite the stress-energy tensor in a more compact way

$$\begin{aligned} \widetilde{T}_{\mu\nu} &= T_{\mu\nu} - \frac{\Lambda}{8\pi G} g_{\mu\nu} \\ &= (\tilde{p} + \tilde{\varrho}) u_\mu u_\nu + \tilde{p} g_{\mu\nu}, \end{aligned} \tag{1.26}$$

so that

$$R_{\mu\nu} - \frac{1}{2} g_{\mu\nu} R = 8\pi G \widetilde{T}_{\mu\nu}. \tag{1.27}$$

In (1.26), the effective pressure $\tilde{p}$ and the effective density $\tilde{\varrho}$ are related to the corresponding quantities for a perfect fluid by

$$\tilde{p} = p - \frac{\Lambda}{8\pi G}, \quad \tilde{\varrho} = \varrho + \frac{\Lambda}{8\pi G}. \tag{1.28}$$

Although after the discovery of the expansion of the Universe in the late 1920s there was no need for a term that made the Universe static, the cosmological constant remained a subject of great interest and it is today the simplest possible explanation for the observed accelerated expansion of the Universe. The standard model of cosmology that incorporates the effects of the cosmological constant is the ΛCDM model.

We now introduce a model involving the cosmological constant which we will encounter again when discussing inflation in chapter 2. The de Sitter Universe is a cosmological model in which the universe is dominated by a positive valued cosmological constant, that suppressed all other matter contributions empty, i.e. $\varrho = 0$ and $p = 0$, and flat ($k = 0$). Under this conditions, from equations (1.28), we get

$$\tilde{p} = -\tilde{\varrho} = -\frac{\Lambda}{8\pi G}, \tag{1.29}$$

which, if replaced in equation (1.13) gives

$$\frac{\dot{a}^2}{a^2} = H^2 = \frac{\Lambda}{3}, \tag{1.30}$$

corresponding to a Hubble parameter constant in time. This equation has a solution of the form

$$a \propto \exp\left(\sqrt{\frac{\Lambda}{3}}t\right), \tag{1.31}$$

which means that the de Sitter model describes a Universe subject to an exponential expansion where test particles move away from each other because of the repulsive gravitational effect of the positive cosmological constant [5].

In the modern interpretation of Λ, the energy density ϱ_Λ and pressure p_Λ found in (1.29) represent the energy density and pressure of the vacuum, which is the ground state of a quantum system. In such a system, the vacuum state does not contain any physical particles but it is characterized by creation and annihilation of virtual particles. Therefore, it is not empty and contributes to the total energy of the system with a non-zero vacuum energy.

1.1.3 Cosmological horizons

The causal structure of the Universe is determined by the propagation of light in the FRW spacetime (1.3). Massless photons move along null geodesics $\mathrm{d}s^2 = 0$, which under the assumption of isotropy, are given by

$$\mathrm{d}s^2 = -c^2\mathrm{d}t^2 + a(t)^2\mathrm{d}\chi^2 = 0. \tag{1.32}$$

The maximum comoving distance covered by light from a zero initial time to a certain time t defines the region of causal connection with a radius

$$\chi(t) \equiv r_\mathrm{p}(t) = \int_0^t \frac{c\mathrm{d}t'}{a(t')}. \tag{1.33}$$

The physical size associated to this quantity is

$$d_\mathrm{p}(t) = a(t)r_\mathrm{p}(t) = a(t)\int_0^t \frac{c\mathrm{d}t'}{a(t')}. \tag{1.34}$$

In equation (1.34), the lower limit of integration taken equal to 0 may lead to the possibility of a divergent integral since also $a(t)$ tends to zero for small t. In this case, an observer O at time

t is in principle in causal connection with the whole Universe. On the other hand, if the integral in equation (1.34) converges to a finite value in this limit, then the observer at O can receive light signals from regions within a spherical surface of radius $d_{\rm p}(t)$. Any source of light located at a proper distance $d > d_{\rm p}(t)$ in the interval of time $[0, t]$ cannot possibly reach the observer O. In this case, the radius $d_{\rm p}(t)$ is called the particle horizon at time t of the observer.

In the standard FRW models where $a(t) \propto t^{\alpha}$, with $\alpha = \frac{2}{3(1+w)}$, the particle horizon (1.34) is approximately given by

$$d_{\rm p}(t) \sim \frac{3(1+w)}{1+3w} ct \tag{1.35}$$

under the condition $w \geq -1/3$, otherwise the integral in equation (1.34) would be divergent. Using the fact that the Hubble parameter in FRW models is given by

$$H = \frac{2}{3(1+w)t}, \tag{1.36}$$

then equation (1.35) can be rewritten as

$$d_{\rm p}(t) \sim \frac{2}{1+3w} \frac{c}{H}, \tag{1.37}$$

where this solution corresponds to a decelerated expansion $\ddot{a} < 0$ (see the Friedmann equation (1.12)).

The particle horizon is related to the Hubble radius $R_{\rm H}$, which will play an important role when we discuss inflation. The Hubble radius is the distance from an observer O of an object moving with the cosmological expansion at the velocity of light with respect to O [5]. It is defined using the Hubble expansion law as

$$R_{\rm H} = c\frac{a}{\dot{a}} = \frac{c}{H}, \tag{1.38}$$

and it can be interpreted as the proper distance travelled by light in the characteristic expansion time of the Universe, the Hubble time

$$\tau_{\rm H} = \frac{a}{\dot{a}} = \frac{1}{H}. \tag{1.39}$$

In the standard FRW models the value of $R_{\rm H}$ coincide at least to order of magnitude with $d_{\rm p}(t)$ (1.34). In fact, using equations (1.38) and (1.37)

$$d_{\rm p} \simeq \frac{2}{1+3w} R_{\rm H} \sim R_{\rm H}, \tag{1.40}$$

The key difference between the particle horizon and the Hubble radius is that the former takes account of the entire past history, i.e. the past light cone, of the observer at time t, while the latter describes the causal connection between regions in the Universe at a specific time.

1.2 The Dark Matter problem

In this section we address the problem of the nature of dark matter. According to the ΛCDM model, about 26% of the contents of the Universe is made of non-luminous matter, i.e. matter that does not interact with observable electromagnetic radiation, therefore extremely difficult to

detect with standard astronomical equipment. Historically, this component was introduce to explain observations of galaxy velocity curves. The luminous mass density of a spiral galaxy decreases as one goes from the center to the outer region, therefore from the Kepler's second law one expects the rotation velocities of stars moving around the center of the galaxy to decrease with distance from the center. The predicted velocity curve is in conflict with the observed one. There is in fact strong experimental evidence that the rotation curves of spiral galaxies remains flat well outside the region in which most of the luminous material resides [6, 5]. This discrepancy is resolve once we assume that spiral galaxies are surrounded by large dark matter haloes, whose mass is thought to be between 3 and 10 times the mass of the luminous component of the galaxy.

Other evidences of the presence of dark matter in the Universe are given by the analysis of galaxy clusters, where the gravitational mass that keeps the galaxies in orbits does not coincide with the luminous mass, leading to the need of an additional component; by weak gravitational lensing observations, namely the observation of angular distortions in the positions of galaxies due to the distribution of dark matter around galaxy clusters ; by the power spectrum of temperature anisotropies in the CMB, which would have a different structure in the absence of dark matter. Finally, another strong evidence of dark matter comes from the observed structures that characterized the present Universe. In fact, during the radiation domination epoch density perturbations are washed out by the radiation pressure. Dark matter, however, does not interact with radiation and provides the gravitational potential wells within which gas cools and condenses to form galaxies.

The nature of dark matter is still unknown and many are the proposed candidates, such as baryonic candidates involving neutral hydrogen gas and massive compact halo objects (MACHOs), which are however in strong disagreement with observations, and non-baryonic candidates that invoke hypothetical particles such as axions, sterile neutrinos, weakly interacting massive particles (WIMPs), gravitationally-interacting massive particles (GIMPs), or supersymmetric particles. Nonetheless, these possibilities have found no experimental evidence so far.

Chapter 2

The inflationary mechanism

The standard Hot Big Bang model reviewed in section 1.1 is incomplete since it does not explain why the present Universe is homogeneous and isotropic on large scales without a fine-tuned set of initial conditions and how were generated the seed perturbation that lead to structure formation. In this chapter we explore two of the main problems of the HBB model, the horizon problem and the flatness problem, and we explain how inflation, an early period of accelerated expansion, drives the primordial Universe towards homogeneity and isotropy, even if it starts in a more generic initial state.

In the second part of this chapter, we show how the quantum fluctuations that arise during the inflationary period generate the seeds for the primordial black holes formation.

2.1 The Hot Big Bang Model Problems

Despite the outstanding successes achieved by the standard cosmology (see e.g. Ref. [5]), there remain certain problems remain unsolved. Here we discuss two of them, the horizon problem and the flatness problem.

2.1.1 The horizon problem

In Chapter 1 we introduced the particle horizon $d_{\rm H}(t)$ in equation (1.34) and showed that all the Friedmann models with equation-of-state parameter $w > -1/3$ possess a finite? particle horizon. On the other hand, cosmological principle requires homogeneity and isotropy in regions of the Universe which are outside each other's particle horizons at early times and which, therefore, have never been in causal contact. An example of the isotropy property is the observed isotropy of the Cosmic Microwave Background radiation. The horizon at photon decoupling is only 205 Mpc while its present value is 4000 Mpc, consequently microwaves coming from regions that were outside the horizon at decoupling could have never communicate by causal processes [4]. The inflationary mechanism provides a dynamical mechanisms that explains why these causally-disconnected regions show such similar physical properties.

In section 1.1.3 we showed that the particle horizon coincided with the Hubble radius $R_{\rm H}$ (1.38) at least to order of magnitude. From now on we do not distinguish between them and we shall use the more practical Hubble radius. Its comoving size is given by

$$r_{\rm H} = \frac{c}{\dot{a}} = \frac{c}{aH}, \tag{2.1}$$

therefore, using the time-dependence of the scale factor (1.18) for $w \neq -1$, we see that the Hubble radius changes as

$$\dot{r}_{\rm H} \propto -\ddot{a} \propto (1+3w). \tag{2.2}$$

Clearly, for models with a finite cosmological horizon $\dot{r}_{\rm H} > 0$ hence $\ddot{a} < 0$.

Let us suppose that there exists a period $t_{\rm i} < t < t_{\rm f}$ of the evolution of the Universe during which the Hubble radius suffers a shrinking $\dot{r}_{\rm H} < 0$, namely a period of accelerated expansion $\ddot{a} > 0$. Under this assumption, consider regions with a comoving scale l_0 which is not causally connected before a time $t_1 < t_{\rm i}$, as pictured in Figure 2.1. It becomes causally connected in the interval $t_1 < t < t_2$, with $t_{\rm i} < t_2 < t_{\rm f}$, and leaves the horizon at t_2. After $t_{\rm f}$ the horizon will continue to grow and it will exist a time t_3 when the scale l_0 enters the horizon again.

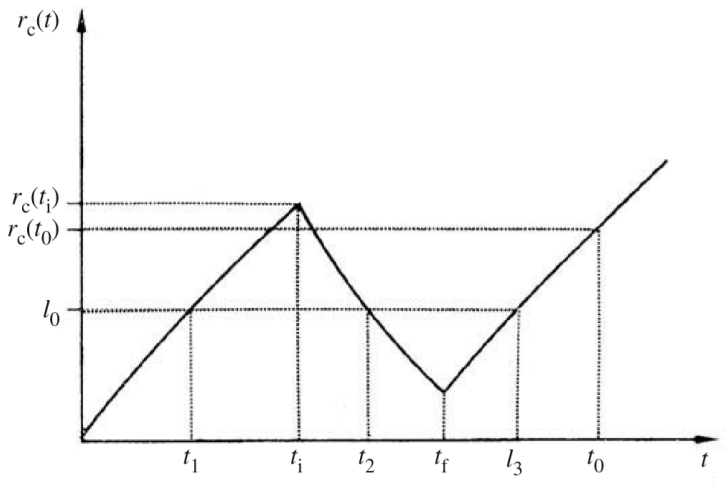

Figure 2.1: Evolution of the comoving cosmological horizon $r_{\rm H}(t)$ assuming a phase of accelerated expansion (inflation) from $t_{\rm i}$ to $t_{\rm f}$ [5].

The horizon problem is then solved if the causal connected scale at the beginning of the expansion is greater than the present scale of the horizon, which means that the period of accelerated expansion has to be long enough for

$$r_{\rm H}(t_{\rm i}) \geq r_{\rm H}(t_0), \tag{2.3}$$

to happen. The duration of inflation can be quantified by means of the numbers of e-folds, defined as

$$\mathcal{N} = \ln\left(\frac{a(t_{\rm f})}{a(t_{\rm i})}\right) = \int_{\rm i}^{\rm f} {\rm d}t'\ H(t'). \tag{2.4}$$

From the requirement in equation (2.3), we obtain a minimum $\mathcal{N}_{\rm min} \approx 60$.

2.1.2 The flatness problem

Observations assert that the present Universe is nearly flat, in other words the present density parameter including the contributions from all components $\Omega_{\rm tot,0} \simeq 1$. Given the definition of the density parameter in equation (1.22) at an arbitrary time t, we can rewrite it using in terms of the comoving Hubble radius (2.1)

$$\Omega(t) - 1 = \frac{k}{(aH)^2} = k\, r_{\rm H}^2, \tag{2.5}$$

where we set $c = 1$. In standard cosmology the comoving Hubble radius grows with time, therefore from equation (2.5) one expects the quantity $|\Omega(t) - 1|$ to grow with time and the geometry of the present Universe to be curved. The near-flatness observed today requires an extreme fine-tuning of $\Omega(t)$ close to the value 1 in the early Universe. This fine-tuning can be estimated as [5]

$$\Omega(t_{\rm P}) \simeq 1 + (\Omega(t_0) - 1)10^{-60}, \tag{2.6}$$

where $t_{\rm P} \approx 10^{-43}$ s is the Planck time and t_0 indicates the present time. The deviation from the flatness at Planck scale in a Universe without inflation should have been of order 10^{-60}.

If we assume that there was a period $t_{\rm i} < t < t_{\rm f}$ in which the Hubble radius decreases with time, then the Universe would be driven towards flatness. As it is shown in Figure 2.2 for an open Universe (a) and closed Universe (b), during the inflationary stage the density parameter $\Omega(t)$ tends to the value 1 and, if the period of accelerated expansion is sufficiently long then the divergence from the flatness should be delayed well beyond the present time t_0. As in the case

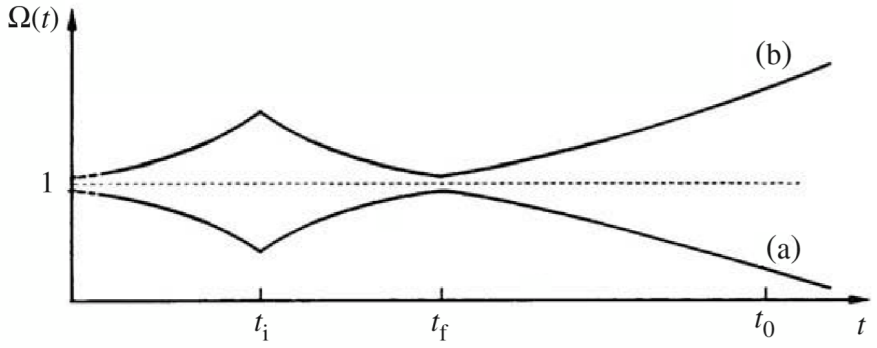

Figure 2.2: Evolution of the $\Omega(t)$ for an open Universe (a) and closed Universe (b) [5].

of the horizon problem, the flatness problem is solved if the period of accelerated expansion is long enough. In terms of the number of e-folds (2.4), again one obtains $\mathcal{N}_{\rm min} \approx 60$.

2.2 The dynamics of inflation

As we saw in section 2.1, a sufficiently long stage of the evolution of the Universe characterized by an accelerated expansion, i.e. inflation, can solve the horizon and the flatness problems. The crucial assumption of the inflationary mechanism is that the observable Universe is far inside the horizon at the beginning of inflation and far outside the horizon at the end of inflation. In this chapter we describe such a mechanism from a theoretical point of view and we explore the main assumptions required for inflation to happen.

Before moving on the quantum field theory description of inflation, we remark the analogy between the de Sitter Universe and the inflationary mechanism. From the Friedmann equation (1.13), we have that the stress-energy tensor associated to the expansion has a negative pressure

$$\frac{\ddot{a}}{a} = -\frac{4\pi G}{3}(\varrho + 3p) > 0 \quad \Rightarrow \quad p < -\frac{\varrho}{3}. \tag{2.7}$$

We encountered a cosmological model with negative pressure when we introduced the de Sitter

model in section 1.1.2, where the scale factor grows exponentially

$$a(t) \propto \mathrm{e}^{\sqrt{\frac{\Lambda}{3}}t}, \tag{2.8}$$

and the expansion is driven by the cosmological constant Λ. In the modern interpretation, Λ is linked to the quantum fluctuations of vacuum. The energy generated by these fluctuations is given by the vacuum expectation value (vacuum expectation value) of the stress-energy tensor

$$\begin{aligned} \langle T_{\mu\nu} \rangle &= -\langle p_\Lambda \rangle g_{\mu\nu}, \\ &= \frac{\Lambda}{8\pi G} g_{\mu\nu}, \end{aligned} \tag{2.9}$$

where we used equations (1.10) and (1.29). Therefore, in this case the vacuum expectation value of the stress-energy tensor acts like the cosmological constant that drives the expansion. This gives a hint of what we should expect from a theory that describes the inflationary mechanism.

In the following we will study the dynamics of a scalar field, the inflaton, which is characterized by a non-zero vacuum expectation value, in the FRW Universe. We will show that it provides the mechanism by which the evolution of the Universe experiences a period of rapid expansion.

2.2.1 The inflaton field and the slow-roll paradigm

The simplest models of inflation involve a single scalar field $\phi(t, \mathbf{x})$, whose Lagrangian is given by

$$\mathcal{L}_\phi = -\frac{1}{2} g^{\mu\nu} \partial_\mu \phi \partial_\nu \phi - V(\phi) \ , \tag{2.10}$$

where the potential $V(\phi)$ describes the self-interactions of the field. The dynamics of the field is governed by the action

$$S_\phi = \int \mathrm{d}^4\mathrm{x} \sqrt{-g} \ \mathcal{L}_\phi[\phi, g_{\mu\nu}]. \tag{2.11}$$

For a complete action describing a scalar field (which we assume minimally coupled to gravity for simplicity) in a curved spacetime we should add the Hilbert-Einstein action

$$\mathcal{S}_{HE}[R] = \frac{1}{16\pi G} \int \mathrm{d}^4\mathrm{x} \sqrt{-g} \ R. \tag{2.12}$$

Moreover, one should include an action for the matter component, i.e. fermions, bosons, which can be described as a fluid, but this can be safely neglected during inflation thanks to the no-hair theorem [5]. In fact, a general property of inflationary Universes is that any inhomogeneity present at the initial time is smoothed out by the expansion.

Replacing the Lagrangian (2.10) in equation (1.9), we derive the stress-energy tensor associated to the inflaton

$$\begin{aligned} T^\phi_{\mu\nu} &= -\frac{2}{\sqrt{-g}} \frac{\delta\sqrt{-g}}{\delta g^{\mu\nu}} \mathcal{L}_\phi - \frac{2}{\sqrt{-g}} \frac{\delta \mathcal{L}_\phi}{\delta g^{\mu\nu}} \sqrt{-g} \\ &= -\frac{2}{\sqrt{-g}} \left(-\frac{1}{2} \sqrt{-g} g_{\mu\nu} \mathcal{L}_\phi \right) + \partial_\mu \phi \partial_\nu \phi \\ &= \partial_\mu \phi \partial_\nu \phi + g_{\mu\nu} \mathcal{L}_\phi. \end{aligned} \tag{2.13}$$

The equation of motion of the inflaton field can be derived from the action in equation (2.11) using the principal of least action and it is given by the Klein-Gordon equation

$$\Box \phi(t, \mathbf{x}) = \frac{\partial V(\phi)}{\partial \phi}, \tag{2.14}$$

where in the left-hand side (LHS) there is the d'Alembertian operator in a curved spacetime

$$\Box\phi = \frac{1}{\sqrt{-g}}\partial_\nu\left[\sqrt{-g}\; g^{\mu\nu}\partial_\mu\phi\right] = g^{\mu\nu}\partial_\mu\partial_\nu\phi - g^{\mu\nu}\Gamma^\varrho_{\mu\nu}\partial_\varrho\phi. \tag{2.15}$$

In the FRW geometry (1.2), the LHS of equation (2.14) becomes

$$\begin{aligned}\frac{1}{\sqrt{-g}}\partial_\nu\left[\sqrt{-g}\; g^{\mu\nu}\partial_\mu\phi\right] &= \frac{1}{a(t)^3}\partial_0\left[a(t)^3\; g^{00}\partial_0\phi\right] + \frac{1}{a(t)^3}\partial_i\left[a(t)^3\; g^{ii}\partial_i\phi\right] \\ &= \frac{1}{a(t)^3}\left[-3a^2\dot{a}\partial_0\phi - a^3\partial_0\partial_0\phi\right] + \frac{1}{a(t)^2}\partial_i\partial_i\phi \\ &= -3H(t)\dot{\phi} - \ddot{\phi} + \frac{1}{a(t)^2}\nabla^2\phi,\end{aligned} \tag{2.16}$$

therefore the equation of motion of the inflaton in the FRW Universe reads as

$$\ddot{\phi} + 3H(t)\dot{\phi} - \frac{1}{a(t)^2}\nabla^2\phi = -\partial_\phi V, \tag{2.17}$$

where the term $3H(t)\dot{\phi}$ is called friction term. It is caused by the expansion of the Universe and it represents the redshift of the momentum $\dot{\phi}$ caused by this expansion.

It is convenient to consider separately two contributions to the scalar field $\phi(t, \mathbf{x})$: the spatially homogeneous background $\phi(t)$ and the quantum fluctuations $\delta\phi(t, \mathbf{x})$

$$\phi(t, \mathbf{x}) = \phi(t) + \delta\phi(t, \mathbf{x}), \tag{2.18}$$

such that

$$\left|\frac{\delta\phi(t, \mathbf{x})}{\phi(t)}\right| \ll 1, \tag{2.19}$$

where the background contribution is the vacuum expectation value of the inflaton

$$\phi(t) = \langle\phi(t, \mathbf{x})\rangle. \tag{2.20}$$

We now restrict our discussion to the study of the dynamics of the background contribution and describe that of the fluctuations in section 2.4.

The contribution of $\phi(t)$ to equation (2.17) reads as

$$\ddot{\phi} + 3H(t)\dot{\phi} + \partial_\phi V = 0, \tag{2.21}$$

and we show that $\phi(t)$. As regards the stress-energy tensor of $\phi(t)$, we have for the energy density

$$\begin{aligned}\varrho_\phi = T^0_0 &= -\partial^0\phi\partial_0\phi + g^0_0\mathcal{L}_\phi \\ &= \dot{\phi}^2 - \left[-\frac{1}{2}(-1)\dot{\phi}^2 - V(\phi)\right] \\ &= \frac{1}{2}\dot{\phi}^2 + V(\phi),\end{aligned} \tag{2.22}$$

and for the pressure density

$$\begin{aligned}p_\phi\delta_{ij} = T^i_j &= \partial^i\phi\partial_j\phi + g^i_i\mathcal{L}_\phi \\ &= \delta^i_j\left[-\frac{1}{2}g^{00}\dot{\phi}^2 - V(\phi)\right] \\ &= \left[\frac{1}{2}\dot{\phi}^2 - V(\phi)\right]\delta^i_j.\end{aligned} \tag{2.23}$$

Putting together the results of equations (2.22) and (2.23), we have that the resulting equation of state is given by

$$w_\phi \equiv \frac{p_\phi}{\varrho_\phi} = \frac{\frac{1}{2}\dot{\phi}^2 - V(\phi)}{\frac{1}{2}\dot{\phi}^2 + V(\phi)}, \tag{2.24}$$

which yields the negative pressure required to have an accelerated expansion in the slow-roll limit

$$\dot{\phi}^2 \ll V(\phi), \tag{2.25}$$

i.e. if the potential energy $V(\phi)$ dominates over the kinetic energy term $(1/2)\dot{\phi}^2$ For a more intuitive point of view, we simplify the system and assume the vacuum expectation value of the inflaton to be constant

$$\bar{\phi} \equiv \langle \phi(t, \mathbf{x}) \rangle. \tag{2.26}$$

Then, the stress-energy tensor become (2.13)

$$T^\phi_{\mu\nu} = -g_{\mu\nu} V(\bar{\phi}). \tag{2.27}$$

Comparing this result to what we found for the cosmological constant in equation (2.9), we see that the potential of the inflaton $V(\phi)$ represents the vacuum energy associated to $\phi(t)$ which drives the accelerated expansion.

The slow-roll condition (2.25) leads to the conclusion that since the kinetic energy of the inflaton has to be extremely low with respect to the potential, the particle moves slowly along it. As a consequence, a good candidate of an inflationary potential should be flat enough to allow the slow-roll of the inflaton and the acceleration of the field should be negligible in equation (2.21). This last condition translates in

$$|\ddot{\phi}| \ll |3H\dot{\phi}|, |\partial_\phi V|, \tag{2.28}$$

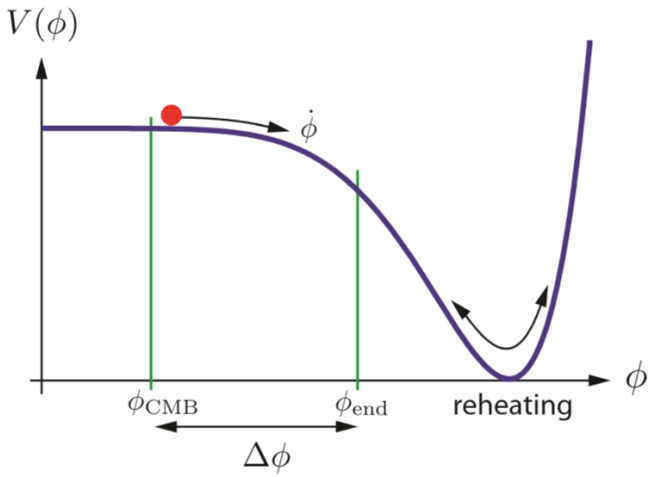

Figure 2.3: A possible shape of the potential for the slow-roll inflation [7].

Using equation (2.28), the equation of motion of inflation (2.21) can be approximated by

$$3H\dot{\phi} \simeq -\partial_\phi V(\phi), \tag{2.29}$$

and the Friedmann equation (1.13) reads as

$$H^2 \simeq \frac{8\pi G}{3} V(\phi), \tag{2.30}$$

Clearly, under the slow-roll regime the Hubble parameter is nearly constant, therefore the evolution of the scale factor is given by the following equation

$$a(t) \propto \mathrm{e}^{Ht}. \tag{2.31}$$

The slow-roll conditions (2.25) and (2.28) necessary for a successful inflation can be parametrized introducing the slow-roll parameters ε and η. The definition of ε is related to the evolution of the Hubble parameter and it is given by

$$\varepsilon \equiv -\frac{\dot{H}}{H^2}. \tag{2.32}$$

In addition to this, ε is also related to the acceleration of a Universe dominated by the inflaton

$$\begin{aligned} \ddot{a} &= \dot{a}H + a\dot{H} = a(H^2 + \dot{H}) \\ &= aH^2\left(1 + \frac{\dot{H}}{H^2}\right) = aH^2(1-\varepsilon). \end{aligned} \tag{2.33}$$

From this result, we have that the period of accelerated expansion occurs as long as $\varepsilon \ll 1$.

We now show that this last requirement is equivalent to the slow-roll condition in equation (2.25), which can be rewritten in another form using equations (2.29) and (2.30). In particular we obtain that

$$\frac{\left(\partial_\phi V(\phi)\right)^2}{V(\phi)} \ll H^2 \quad \Rightarrow \quad \frac{1}{16\pi G}\frac{\partial_\phi V(\phi)^2}{V(\phi)^2} \ll 1. \tag{2.34}$$

We employ equations (2.29) and (2.30) to write ε in an approximate form

$$\begin{aligned} \varepsilon &\simeq -\frac{1}{2}\sqrt{\frac{8\pi G}{3}V(\phi)}\frac{\partial_\phi V(\phi)\dot{\phi}}{H^2} \\ &= \frac{1}{2}\frac{\partial_\phi V(\phi)}{H}\frac{\partial_\phi V(\phi)}{3H} = \frac{1}{16\pi G}\frac{\partial_\phi V(\phi)^2}{V(\phi)^2}, \end{aligned} \tag{2.35}$$

which is clearly equivalent to the slow-roll condition in equation (2.34).

The second slow-roll parameter η is defined as

$$\eta \equiv \frac{1}{3}\frac{\partial_\phi^2 V}{H^2}, \tag{2.36}$$

which can be further rewritten in the following form

$$\eta \simeq \frac{1}{3}\frac{\partial_\phi^2 V}{\frac{8\pi G}{3}V} = \frac{1}{8\pi G}\frac{\partial_\phi^2 V}{V}, \tag{2.37}$$

where we used equation (2.30).

Consider now the condition $|\ddot{\phi}| \ll |\partial_\phi V|$, it can be shown that it is equivalent to requiring $|\eta| \ll 1$. In fact, deriving both sides we get

$$3H\ddot{\phi} \simeq \partial_\phi^2 V(\phi)\dot{\phi} \quad \Rightarrow \quad \ddot{\phi} \simeq \frac{\partial_\phi^2 V(\phi)\dot{\phi}}{3H} \ll 3H\dot{\phi}, \tag{2.38}$$

which, being $H \simeq$ constant during inflation, leads to the condition

$$\frac{\partial_\phi^2 V}{H^2} \ll 1. \tag{2.39}$$

In conclusion, the slow-roll approximation given in equations (2.25) and (2.28) imply the conditions (2.34) and (2.36) on the flatness of the inflationary potential.

2.3 Inflationary models

In our previous discussion, we did not specify the shape of the inflationary potential which determines the dynamics of the inflaton field. In the framework of single-field inflation, the different possibilities for $V(\phi)$ can be classified using the difference between the inflaton at the time when CMB fluctuations were created at $\phi_{\rm cmb}$ to the end of inflation at $\phi_{\rm end}$

$$\Delta\phi = \phi_{\rm cmb} - \phi_{\rm end}, \tag{2.40}$$

measured in Planck units. In this section, we briefly review the main models.

Small-Field Inflation In small-field models $\Delta\phi < M_{\rm P}$, which means that the inflaton has a small variation, called sub-Planckian. The correspondent potential can be locally approximated by

$$V(\phi) = V_0 \left[1 - \left(\frac{\phi}{\mu}\right)^p\right] + \dots, \tag{2.41}$$

where the dots represent higher-order terms that become important near the end of inflation [7]. This kind of model arises typically in mechanisms of spontaneous symmetry breaking, where the field rolls off an unstable equilibrium toward a displaced vacuum.

Large-Field Inflation In such models we have $\Delta\phi > M_{\rm P}$, namely the field evolution is super-Planckian. The inflaton starts with large values and then moves towards a minimum at the origin $\phi = 0$. The typical large-field model is *chaotic inflation* characterized by

$$V(\phi) \propto \phi^{\rm p}. \tag{2.42}$$

2.4 Cosmological perturbations from inflation

We think that cosmological perturbations have their origin in the quantum fluctuations that arise during inflation. In section 2.2, we explored the dynamics of the homogeneous inflaton field in the expanding Universe using the decomposition in equation (2.18). In this section, we focus on the effects of quantum fluctuations $\delta\phi(t, \vec{x})$ around the background evolution $\phi(t)$. We will show that they constitute the seed of the inhomogeneities in the present Universe.

2.4.1 Dynamics of quantum fluctuations: qualitative solution

In this section, we give a qualitative overview of the solutions to give a basic understanding of the physics behind the dynamics of quantum fluctuations.

The Klein-Gordon equation for the quantum fluctuations is given by

$$\ddot{\delta\phi} + 3H\dot{\delta\phi} - \frac{1}{a^2}\nabla^2\delta\phi = -\partial_\phi V(\phi(t))\delta\phi. \tag{2.43}$$

It is convenient to go to the Fourier space, where we rewrite the fluctuations as a superposition of plane waves of wavenumber k

$$\delta\phi(t,\mathbf{x}) = \frac{1}{(2\pi)^3}\int \mathrm{d}^3k\; e^{i\mathbf{k}\cdot\mathbf{x}}\delta\phi_{\mathbf{k}}(t), \tag{2.44}$$

where this decomposition is valid only in a flat spacetime, which is a reasonable assumption during inflation. Since $\delta\phi(t,\mathbf{x})$ is real, we have that $(\delta\phi_{\mathbf{k}})^* = \delta\phi_{-\mathbf{k}}$.

In Fourier space, equation (2.43) becomes

$$\ddot{\delta\phi}_{\mathbf{k}} + 3H\dot{\delta\phi}_{\mathbf{k}} + \frac{1}{a^2}k^2\delta\phi_{\mathbf{k}} = -\partial_\phi^2 V\delta\phi_{\mathbf{k}}. \tag{2.45}$$

In order to simplify the problem, we consider a massless scalar field, i.e. $\partial_\phi^2 V \approx 0$, which corresponds to the requirement of a small η parameter

$$\eta = \frac{1}{3}\frac{\partial_\phi^2 V}{H^2} \ll 1. \tag{2.46}$$

Under this assumption, equation (2.45) approximates as

$$\ddot{\delta\phi}_{\mathbf{k}} + 3H\dot{\delta\phi}_{\mathbf{k}} + \frac{1}{a^2}k^2\delta\phi_{\mathbf{k}} \simeq 0. \tag{2.47}$$

We distinguish between two regimes depending on the comoving wavelength of the fluctuations

$$\lambda_{\mathrm{phys}} \simeq \frac{2\pi}{k_{\mathrm{phys}}} = a(t)\lambda_{\mathrm{com}}, \tag{2.48}$$

that is the sub-horizon regime if λ is smaller than the Hubble horizon radius (2.1)

$$\lambda \ll \frac{1}{aH} \quad \Rightarrow \quad \frac{k}{aH} \gg 1, \tag{2.49}$$

and the super-horizon regime when λ is greater than the Hubble horizon radius

$$\lambda \gg \frac{1}{aH} \quad \Rightarrow \quad \frac{k}{aH} \ll 1. \tag{2.50}$$

Sub-horizon regime

In this regime, we show that we can neglect the friction term. In fact, in Fourier space such reads as

$$3H\dot{\delta\phi}_{\mathbf{k}} \simeq 3H^2\delta\phi_{\mathbf{k}}, \tag{2.51}$$

where we used the Hubble time scale $\tau_{\rm H} = H^{-1}$ as the time reference. Comparing this result with the Fourier transform of the Laplacian term in equation (2.97) in the sub-horizon regime $k \gg aH$ we obtain the following relation

$$3H^2\delta\phi_{\mathbf{k}} \ll \frac{1}{a^2}k^2\delta\phi_{\mathbf{k}}, \tag{2.52}$$

therefore (2.47) becomes

$$\ddot{\delta\phi}_{\mathbf{k}} + \frac{1}{a^2}k^2\delta\phi_{\mathbf{k}} \simeq 0. \tag{2.53}$$

This is an harmonic oscillator equation with a time dependant frequency given by the factor $k/a(t)$. In conclusion, we have found that in the sub-horizon regime the Fourier transformed quantum fluctuations $\delta\phi_{\mathbf{k}}$ oscillate with an amplitude which decays with time as $a(t)^{-2}$ (see equation (2.31)), which is not unexpected knowing that at small scales, such as those inside the horizon, we locally recover the flat Minkowski spacetime where the expansion of the Universe is negligible.

Super-horizon regime

In this regime, we proceed as in the sub-horizon regime and see that

$$3H^2\delta\phi_{\mathbf{k}} \gg \frac{1}{a^2}k^2\delta\phi_{\mathbf{k}}, \tag{2.54}$$

namely in this case the friction term is dominant with respect to the Laplacian term. Therefore, equation (2.47) becomes

$$\ddot{\delta\phi}_{\mathbf{k}} + 3H\dot{\delta\phi}_{\mathbf{k}} \simeq 0, \tag{2.55}$$

a second order linear differential equation, whose solution is given by

$$\delta\phi_{\mathbf{k}} = A + Be^{-3Ht}. \tag{2.56}$$

After an opportune amount of time, the exponential term decays and the fluctuations freeze out. There is an intuitive way to understand the physics behind this result. In fact we are considering fluctuations much bigger than the Hubble horizon, which gives the maximum distance of casual connection between events (for more details see section 1.1.3). Therefore, fluctuations bigger than that cannot interact nor grow. We are interested in finding out the amplitude of the fluctuations which, as we shall see, connects the theoretical results with observations.

2.4.2 Dynamics of quantum fluctuations: exact solution

We can now focus on a more exact solution that includes quantum field theory effects and the mass term given by $\partial^2_\phi V$. As done in the previous section, we explore the solution in the sub-horizon and super-horizon limit.

We first introduce the operator $\widehat{\delta\phi}(\tau, \mathbf{x})$ defined as

$$\widehat{\delta\phi}(\tau, \mathbf{x}) = a(\tau)\delta\phi(\tau, \mathbf{x}), \tag{2.57}$$

where we use the conformal time τ (1.5) instead of the cosmic time. Then, $\widehat{\delta\phi}(\tau, \mathbf{x})$ can be written as a linear combination of the creation-annihilation operators $(a_{\mathbf{k}}, a^\dagger_{\mathbf{k}})$

$$\widehat{\delta\phi}(\tau, \mathbf{x}) = \frac{1}{(2\pi)^3}\int \mathrm{d}^3\mathrm{k}\, \left[u_{\mathbf{k}}(\tau)a_{\mathbf{k}}\, e^{i\mathbf{k}\cdot\mathbf{x}} + u^*_{\mathbf{k}}(\tau)a^\dagger_{\mathbf{k}}\, e^{-i\mathbf{k}\cdot\mathbf{x}}\right], \tag{2.58}$$

and time-dependant mode functions $u_{\mathbf{k}}(\tau)$ obey a normalization condition

$$u'^{*}_{\mathbf{k}}(\tau)u_{\mathbf{k}}(\tau) - u^{*}_{\mathbf{k}}(\tau)u'_{\mathbf{k}}(\tau) = i, \tag{2.59}$$

such that commutation rules are given by

$$\begin{aligned} [a_{\mathbf{k}}, a_{\mathbf{k}'}] &= [a^{\dagger}_{\mathbf{k}}, a^{\dagger}_{\mathbf{k}'}] = 0, \\ [a_{\mathbf{k}}, a^{\dagger}_{\mathbf{k}'}] &= \hbar\delta^{(3)}(\mathbf{k}-\mathbf{k}'). \end{aligned} \tag{2.60}$$

We know that in the Minkowski spacetime, mode functions are described by plane waves such as

$$u_{\mathbf{k}}(\tau) \sim \frac{e^{-i\omega_{\mathbf{k}}\tau}}{\sqrt{2\omega_{\mathbf{k}}}}\,, \quad \omega_{\mathbf{k}} = \sqrt{k^2+m^2}. \tag{2.61}$$

However, in a curved spacetime, as the expanding FRW Universe, we expect a more complicated expression for $u_{\mathbf{k}}(\tau)$. As a matter of fact, in quantum field theory on curved spacetime there is an ambiguity with the choice of the vacuum state, therefore $u_{\mathbf{k}}(\tau)$ is not a priori fixed. We employ the Bunch-Davies condition on the vacuum state, which states that in the limit of small scales and for initial times the mode functions $u_{\mathbf{k}}(\tau)$ are given by equation (2.61).

Before rewriting equation (2.45) in the Fourier space, we explicitly change time coordinate going from the reference time t to the conformal time τ such that

$$\frac{d}{dt} \quad \longrightarrow \quad \frac{d}{dt}\frac{d\tau}{d\tau} = \frac{1}{a}\frac{d}{d\tau} \tag{2.62}$$

We perform the calculations term by term using the coordinate change in equation (2.62). On the left-hand side of equation (2.45) we have

$$\begin{aligned} \ddot{\delta\hat{\phi}}_{\mathbf{k}} &= \frac{1}{a}\frac{d}{d\tau}\left[\frac{1}{a}\frac{d}{d\tau}\left(\frac{\delta\hat{\phi}_{\mathbf{k}}}{a}\right)\right] \\ &= \frac{1}{a}\frac{d}{d\tau}\left[\frac{1}{a}\left(\frac{\delta\hat{\phi}'_{\mathbf{k}}}{a} - \frac{a'}{a^2}\delta\hat{\phi}_{\mathbf{k}}\right)\right] \\ &= \frac{1}{a}\left(\frac{\delta\hat{\phi}''_{\mathbf{k}}}{a^2} - 2\frac{a'}{a^3}\delta\hat{\phi}'_{\mathbf{k}} - \frac{a''}{a^3}\delta\hat{\phi}_{\mathbf{k}} - 3\frac{a'^2}{a^4}\delta\hat{\phi}_{\mathbf{k}} - \frac{a'}{a^3}\delta\hat{\phi}'_{\mathbf{k}}\right) \\ &= \frac{\delta\hat{\phi}''_{\mathbf{k}}}{a^3} - 2\frac{a'}{a^4}\delta\hat{\phi}'_{\mathbf{k}} - \frac{a''}{a^4}\delta\hat{\phi}_{\mathbf{k}} + 3\frac{a'^2}{a^5}\delta\hat{\phi}_{\mathbf{k}} - \frac{a'}{a^4}\delta\hat{\phi}'_{\mathbf{k}}, \end{aligned} \tag{2.63}$$

and

$$\begin{aligned} 3H\dot{\delta\hat{\phi}}_{\mathbf{k}} &= 3\frac{1}{a^2}\frac{da}{d\tau}\frac{1}{a}\frac{d}{d\tau}\left(\frac{\delta\hat{\phi}_{\mathbf{k}}}{a}\right) \\ &= 3\frac{a'}{a^4}\delta\hat{\phi}'_{\mathbf{k}} - 3\frac{a'^2}{a^5}\delta\hat{\phi}_{\mathbf{k}}. \end{aligned} \tag{2.64}$$

Finally, putting all the results together, we obtain

$$\delta\hat{\phi}''_{\mathbf{k}} - \frac{a''}{a}\delta\hat{\phi}_{\mathbf{k}} + k^2\delta\hat{\phi}_{\mathbf{k}} = -\partial^2_{\phi}Va^2\delta\hat{\phi}_{\mathbf{k}}, \tag{2.65}$$

which in terms of the mode functions becomes

$$u''_{\mathbf{k}}(\tau) + \left(k^2 - \frac{a''}{a} + \partial^2_{\phi}Va^2\right)u_{\mathbf{k}}(\tau) = 0. \tag{2.66}$$

We find another equation for an harmonic oscillator with time-dependent coefficients. Let us look at the behaviour of the mode function in the sub-horizon and super-horizon regimes for a de Sitter Universe and a quasi-de Sitter Universe.

Solution in de Sitter

In this case, we assume that the inflaton is massless ($\partial_\phi^2 V = 0$) and the de Sitter phase fully describes inflation, i.e. $\varepsilon \to 0$ and $H =$ constant. Under these conditions the conformal time (1.5) is given by

$$d\tau = \frac{dt}{a(t)} = dt\, e^{-Ht}, \tag{2.67}$$

where we used equation (2.31). After integration we obtain

$$\tau = -\frac{1}{H} e^{-Ht} = -\frac{1}{aH}, \tag{2.68}$$

which plugged in equation (2.66) gives

$$u_{\mathbf{k}}''(\tau) + \left(k^2 - 2a^2H^2\right) u_{\mathbf{k}}(\tau) = 0. \tag{2.69}$$

In the sub-horizon limit $k \gg aH$, equation (2.69) becomes

$$u_{\mathbf{k}}''(\tau) + k^2 u_{\mathbf{k}}(\tau) = 0 \quad \Rightarrow \quad u_{\mathbf{k}}(\tau) = \frac{e^{-ik\tau}}{\sqrt{2k}} \tag{2.70}$$

where we chose the Bunch-Davies vacuum state. As predicted in the qualitative analysis given in section 2.4.1, the behaviour of quantum fluctuations of the inflaton are approximated by the usual flat spacetime quantum field theory.

In the super-horizon regime $k \ll aH$, equation (2.69) approximates as

$$u_{\mathbf{k}}''(\tau) - \frac{a''}{a} u_{\mathbf{k}}(\tau) = 0, \tag{2.71}$$

whose solution is simply given by

$$u_{\mathbf{k}}(\tau) = B(k)a(\tau) + C(k)a(\tau)^{-2}. \tag{2.72}$$

Since the second term on the right hand side decays in time as $a(\tau)^{-2}$, the amplitude of the fluctuation reads as

$$|\delta\phi_{\mathbf{k}}| \simeq \frac{|u_{\mathbf{k}}|}{a(\tau)} = |B(k)|, \tag{2.73}$$

which is indeed constant in time beyond the horizon, as predicted in section 2.4.1. Since we are interested in studying perturbations on cosmological scales, $|B(k)|$ represents a link between quantum perturbations at horizon exit time during inflation and perturbations at horizon re-entering time during radiation or matter dominated eras. We thus evaluate $|B(k)|$ at the time of horizon crossing during inflation, denoted with an index I, by matching the sub-horizon and the super-horizon regimes

$$\left.\frac{e^{-ik\tau}}{a\sqrt{2k}}\right|_{k_{\rm I}=(aH)} \equiv B(k) \quad \Rightarrow \quad B(k) = \frac{i}{a\sqrt{2k}}, \tag{2.74}$$

that leads to

$$|\delta\phi_{\mathbf{k}}| = \frac{H_{\rm I}}{\sqrt{2k^3}}, \tag{2.75}$$

where we used $k_{\rm I} = (aH)$.

As shown above, the physics beneath the horizon, at small scales, is the one of special relativity and the quantum fluctuations around the vacuum expectation value of the scalar field were treated according to quantum field theory in a flat spacetime. The mean value of these fluctuations is zero since by definition the vacuum state is characterized by creation and annihilation of particles and a net number of particles equal to zero. As the comoving Hubble radius $r_{\rm H}(t)$ (2.1) shrinks, the rapid expansion stretches the wavelength of the quantum fluctuations in such a way that all fluctuations generated at sub-horizon scales exit the horizon. Here, their amplitude cannot not be affected by causal contact therefore they freeze. After inflation, the comoving horizon starts to grow again, so eventually all fluctuations re-enter the horizon with an imprinting of the primordial fluctuations generated by inflation but with a much larger physical wavelength.

Solution in quasi-de Sitter

Here, we keep the assumption of a massless scalar field but we assume that the expansion is described by a quasi-de Sitter stage, therefore $\varepsilon \neq 0$ but still small.

Using the slow-roll parameters defined in equations (2.32) and (2.36), we rewrite the equation (2.66) in the form of a Bessel equation. In fact, the term a''/a becomes

$$\frac{a''}{a} = \frac{2}{\eta^2}\left(1 + \frac{3}{2}\varepsilon + \mathcal{O}(\varepsilon^2, \eta^2)\right), \tag{2.76}$$

which replaced in the massless approximation of equation (2.66) gives

$$u''_{\mathbf{k}}(\tau) + \left(k^2 - \frac{\nu^2 - 1/4}{\eta^2}\right) u_{\mathbf{k}}(\tau) \simeq 0, \tag{2.77}$$

where we defined $\nu^2 = 9/4 + 3\varepsilon$. Assuming ν constant, a generic solution of equation (2.77) given by

$$u_{\mathbf{k}} = \sqrt{-\tau}\left[c_1(k) H_\nu^{(1)}(-k\tau) + c_2(k) H_\nu^{(2)}(-k\tau)\right], \tag{2.78}$$

with $H_\nu^{(1)}$ and $H_\nu^{(2)}$ are the Henkel function of first and second kind.

In the sub-horizon limit $-k\tau \gg 1$, equation (2.78) can be approximated as

$$u_{\mathbf{k}}(\tau) \simeq \frac{\sqrt{\pi}}{2} \mathrm{e}^{i(\nu+\pi/4)} \sqrt{-\tau} H_\nu^{(1)}(-k\tau), \tag{2.79}$$

whereas in the super-horizon limit $-k\tau \ll 1$ we have

$$u_{\mathbf{k}}(\tau) \simeq \frac{2^{\nu-\frac{3}{2}}}{\sqrt{2k}} \mathrm{e}^{i(\nu+\pi/4)} \left(\frac{\Gamma(\nu)}{\Gamma(3/2)} (-k\tau)^{\frac{1}{2}-\nu}\right). \tag{2.80}$$

Going back to the field fluctuation we obtain the following solution

$$|\delta\phi_{\mathbf{k}}| \simeq 2^{\nu-\frac{3}{2}} \left(\frac{\Gamma(\nu)}{\Gamma(3/2)}\right) \frac{H}{\sqrt{2k^3}} \left(\frac{k}{aH}\right)^{\frac{3}{2}-\nu}. \tag{2.81}$$

Notice that ν can be expanded as

$$\nu = \sqrt{\frac{9}{4} + 3\varepsilon} = \frac{3}{2}\left(1 + \frac{4}{3}\varepsilon\right) \simeq \frac{3}{2} + \varepsilon, \tag{2.82}$$

therefore in the limit $\varepsilon \ll 1$, equation (2.81) can be approximated as

$$|\delta\phi_{\mathbf{k}}| \simeq \frac{H}{\sqrt{2k^3}}\left(\frac{k}{aH}\right)^{-\varepsilon}. \tag{2.83}$$

We recover the solution (2.75) found in the de Sitter case by putting $\varepsilon = 0$.

2.5 The power spectrum

In this section we introduce some fundamental aspects of the statistical properties of a perturbation in order to connect theoretical prediction with observations.

Let us consider a Gaussian random field $\delta(t, \mathbf{x})$ that describes a generic fluctuation in a point of the spacetime. It could be for example the fluctuation of the density field. The statistical properties of such a field are determined by an infinite set of correlation functions defined as

$$\begin{aligned}
&\langle \delta(t, \mathbf{x}_1)\delta(t, \mathbf{x}_2)\rangle = \xi(\mathbf{x}_1, \mathbf{x}_2),\\
&\langle \delta(t, \mathbf{x}_1)\delta(t, \mathbf{x}_2)\delta(t, \mathbf{x}_3)\rangle = \xi(\mathbf{x}_1, \mathbf{x}_2, \mathbf{x}_3),\\
&\vdots\\
&\langle \delta(t, \mathbf{x}_1)\delta(t, \mathbf{x}_2)\ldots\delta(t, \mathbf{x}_N)\rangle = \xi(\mathbf{x}_1, \mathbf{x}_2, \ldots, \mathbf{x}_N),
\end{aligned} \tag{2.84}$$

where the $\langle\cdot\rangle$ symbol refers to the ensemble average.

Gaussian processes are determined only by the *two-point correlation function*, i.e. the first definition in equation (2.84). In fact, the correlation function for odd value of N are null, whereas those characterized by even N can be written as a combination of $\xi(\mathbf{x}_1, \mathbf{x}_2)$. Since the Universe is homogeneous and isotropic, we expect the two-point correlation function to depend only on the relative distance $\xi(r) = \xi(|\mathbf{x}_1 - \mathbf{x}_2|)$.

Knowing that the Fourier transform of the fluctuation reads as

$$\delta(t, \mathbf{x}) = \frac{1}{(2\pi)^3}\int \mathrm{d}^3k\; e^{i\mathbf{k}\cdot\mathbf{x}}\delta_{\mathbf{k}}(t), \tag{2.85}$$

we define the power spectrum $P(k)$ as

$$\langle \delta_{\mathbf{k}_1}(t)\delta_{\mathbf{k}_2}(t)\rangle = (2\pi)^3\delta^{(3)}(\mathbf{k}_1 + \mathbf{k}_2)P(k), \tag{2.86}$$

and we show that the power spectrum is the Fourier transform of the two-point correlation function $\xi(r)$. In fact

$$\begin{aligned}
\xi(r) &= \langle \delta(t, x + r)\delta(t, x)\rangle\\
&= \langle \frac{1}{(2\pi)^3}\int \mathrm{d}^3k\; e^{i\mathbf{k}\cdot(\mathbf{x}+\mathbf{r})}\delta_{\mathbf{k}}(t)\frac{1}{(2\pi)^3}\int \mathrm{d}^3k'\; e^{i\mathbf{k}'\cdot\mathbf{x}}\delta_{\mathbf{k}'}(t)\rangle\\
&= \frac{1}{(2\pi)^6}\int \mathrm{d}^3k\;\int \mathrm{d}^3k'\; e^{i\mathbf{k}\cdot(\mathbf{x}+\mathbf{r})}e^{i\mathbf{k}'\cdot\mathbf{x}}\langle\delta_{\mathbf{k}}(t)\delta_{\mathbf{k}'}(t)\rangle\\
&= \frac{1}{(2\pi)^3}\int \mathrm{d}^3k\;\int \mathrm{d}^3k'\; e^{i\mathbf{k}\cdot(\mathbf{x}+\mathbf{r})}e^{i\mathbf{k}'\cdot\mathbf{x}}\delta^{(3)}(\mathbf{k} + \mathbf{k}')P(k)\\
&= \frac{1}{(2\pi)^3}\int \mathrm{d}^3k\; e^{i\mathbf{k}\cdot\mathbf{r}}P(k).
\end{aligned} \tag{2.87}$$

Another relevant quantity is the variance of the fluctuations defined as

$$\sigma^2 \equiv \langle \delta_{\rm k}^2 \rangle = \frac{1}{(2\pi)^3} \int {\rm d}^3k \; P(k). \tag{2.88}$$

We further introduce the dimensionless power spectrum

$$\mathcal{P}(k) \equiv \frac{k^3}{2\pi^2} P(k), \tag{2.89}$$

by which equation (2.88) becomes

$$\sigma^2 = \int_0^\infty \frac{{\rm d}k}{k} \mathcal{P}(k). \tag{2.90}$$

The scale dependence of $\mathcal{P}(k)$ is given by the spectral index

$$n(k) - 1 = \frac{d \ln \mathcal{P}(k)}{d \ln k}. \tag{2.91}$$

If the spectral index is scale-invariant, i.e. $n(k) = \text{const}$, then the power spectrum $\mathcal{P}(k)$ can be generally written as

$$\mathcal{P}(k) = \mathcal{P}(k_0) \left(\frac{k}{k_0} \right)^{n-1}, \tag{2.92}$$

where k_0 is a pivot scale. We distinguish between different classes of power spectra based on the spectral index: if $n(k) = 1$, then the power spectrum is the so-called Harrison-Zel'dovich power spectrum and it does not depend on the cosmological scale k; if $n(k) > 1$ then we have a blue tilted power spectrum, namely perturbations have more power on small scales than on large scales; on the contrary the red tilted power spectrum has $n(k) < 1$ which means less power on small scales compared to large scales.

The power spectrum of the fluctuations of the inflaton field at lowest order in the slow-roll parameters. Using the fact that $\delta\phi_{\mathbf{k}}(t)^* = \delta\phi_{-\mathbf{k}}(t)$ and that it can be written as a combination of creation-annihilation operators, we obtain

$$\langle \delta\phi_{\mathbf{k}}(t) \delta\phi^*_{\mathbf{k}'}(t) \rangle = (2\pi)^3 \delta^{(3)}(\mathbf{k} - \mathbf{k}') |\delta\phi_{\mathbf{k}}|^2. \tag{2.93}$$

Comparing this result with equation (2.86) we have that

$$P_{\delta\phi}(k) = |\delta\phi_{\mathbf{k}}(t)|^2, \quad \mathcal{P}_{\delta\phi}(k) = \frac{k^3}{2\pi^2} |\delta\phi_{\mathbf{k}}|^2. \tag{2.94}$$

In particular, using the result in (2.75) we find that at super-horizon scales the power spectrum reads as

$$\mathcal{P}_{\delta\phi}(k) = \left(\frac{H}{2\pi} \right)^2 \left(\frac{k}{aH} \right)^{3-2\nu}. \tag{2.95}$$

2.6 From quantum to cosmological fluctuations

In section 2.4 we showed that fluctuations $\delta\phi$ of the inflaton field arise at sub-horizon scale and are stretched by the rapid expansion of the Universe until they exit the horizon and freeze at super-horizon scale. At later times, this fluctuations re-enter the region of causal connection and

interact through physical processes. In this section we examine how the quantum perturbations that have occurred during inflation are related to the primordial density perturbations that constitute the seeds of the present cosmic structure.

During inflation, the fluctuations $\delta\phi$ generate fluctuations in the expansion of the Universe such that different regions will end inflation at slightly different times. To show this, recall the equation of motion of the homogeneous inflaton field (2.21). If we derive with respect to the cosmic time

$$\dddot{\phi} + 3H\ddot{\phi} = -\partial_\phi^2 V(\phi)\dot{\phi} \quad \Rightarrow \quad (\dot{\phi})\ddot{} + 3H(\dot{\phi})\dot{} = -\partial_\phi^2 V(\phi)\dot{\phi}, \tag{2.96}$$

we notice that the resulting equation has the same form of equation (2.43) except for the Laplacian term. In the limit where this term can be neglected, $\delta\phi$ and $\dot{\phi}$ obey to the same equation. In particular, taking the Fourier transform of the Laplacian term

$$\frac{1}{a^2}\nabla^2(\delta\phi) \xrightarrow{\mathcal{F}} -\frac{k^2}{a^2}\delta\phi_{\vec{k}}, \tag{2.97}$$

we have that it vanishes in the limit of large scales, i.e. for k that tends to 0. This corresponds to a coarse-graining process that we will assume valid throughout the following discussion.

In order to study this system, we employ the Wronskian operator, which, given a differential equation and a set of solutions, allows to determine if such solutions are linearly independent or linearly dependent. Given two homogeneous fields $\varphi(t)$ and $\psi(t)$, the Wronskian is defined as

$$W(\varphi,\psi) = \dot{\varphi}\psi - \dot{\psi}\varphi \begin{cases} \neq 0 & \text{two linearly independent solutions,} \\ = 0 & \text{two linearly dependent solutions.} \end{cases} \tag{2.98}$$

In our case, the Wronskian has the following form

$$W(\delta\phi,\dot{\phi}) = (\dot{\delta\phi})\dot{\phi} - \ddot{\phi}\delta\phi. \tag{2.99}$$

If we further derive with respect to time, we obtain that

$$\begin{aligned} \dot{W}(\delta\phi,\dot{\phi}) &= (\ddot{\delta\phi})\dot{\phi} + (\dot{\delta\phi})\ddot{\phi} - \dddot{\phi}\delta\phi - \ddot{\phi}\dot{\delta\phi} \\ &= -3H(\dot{\delta\phi})\dot{\phi} - \partial_\phi V'(\phi(t)\delta\phi\dot{\phi} + 3H\ddot{\phi}\delta\phi + \partial_\phi V'(\phi)\dot{\phi}\delta\phi \\ &= 3H[\ddot{\phi}\delta\phi - (\dot{\delta\phi})\dot{\phi}] \\ &= -3HW(\delta\phi,\dot{\phi}), \end{aligned} \tag{2.100}$$

which has solution decaying with time given by

$$W(\delta\phi,\dot{\phi}) = e^{-3Ht}, \tag{2.101}$$

Thus, using the conditions (2.98), at large scales $\delta\phi$ and $\dot{\phi}$ are related. In particular

$$\delta\phi(t,\mathbf{x}) \propto \dot{\phi} \quad \Rightarrow \quad \delta\phi(t,\mathbf{x}) \simeq (-\delta t(\mathbf{x}))\dot{\phi}, \tag{2.102}$$

where the proportional constant $-\delta t(\mathbf{x})$ has the dimensionality of time and $\mathbf{x}$ represents a large region of the Universe. To simplify the system, we consider a linear dependence on time for the inflaton field given by $\phi(t) = \phi_* \cdot t$, hence $\delta\phi(t,\vec{x}) \simeq (-\delta t(\vec{x}))\phi$ and the decomposition of the scalar field (2.18) becomes

$$\begin{aligned} \phi(t,\mathbf{x}) &= \phi(t) + \delta\phi(t,\mathbf{x}) \\ &\simeq \phi[t - \delta t(\mathbf{x})]. \end{aligned} \tag{2.103}$$

The inflaton field is subject to a temporal shift given by

$$\delta t(\mathbf{x}) \simeq -\frac{\delta\phi(t,\mathbf{x})}{\dot{\phi}(t)}. \tag{2.104}$$

which corresponds to a local time delay in the time at which inflation ends. As a consequence, also the expansion of the Universe is different in different parts of the Universe. We introduce the fluctuations in the number of e-folds $\mathcal{N}$ (2.4) given by the primordial curvature perturbation ζ

$$\zeta = \delta\mathcal{N} = H\delta t \simeq -H\frac{\delta\phi}{\dot{\phi}}, \tag{2.105}$$

where in the last passage we used (2.104). We now show that during inflation the primordial curvature perturbation induce fluctuations in the density field. Let us consider the expression of ϱ in equation (2.22), then

$$\begin{aligned} -H\frac{\delta\varrho}{\dot{\varrho}} &\simeq -H\frac{\partial_\phi V(\phi)\delta\phi}{-3H(\varrho+p)}, \\ &\simeq H\frac{3H\dot{\phi}\delta\phi}{-3H\dot{\phi}^2} \simeq -H\frac{\delta\phi}{\dot{\phi}}, \end{aligned} \tag{2.106}$$

where in the first passage we used the continuity equation (1.15) during inflation. Therefore, $\zeta \simeq -H\delta\varrho/\dot{\varrho}$. An important property of ζ is that it remains constant outside the horizon for adiabatic matter perturbations [8]. Therefore, given a scale k, we can evaluate ζ at the time of horizon crossing $t(k)_{\rm exit}$, knowing that it maintains the same value until it re-enter the horizon at $t(k)_{\rm en}$ during radiation or matter domination.

The power spectrum of the curvature perturbation can be derived using equation (2.105)

$$\mathcal{P}_\zeta \simeq \frac{H^2}{\dot{\phi}^2}\mathcal{P}_{\delta\phi} = \left(\frac{H}{2\pi\dot{\phi}}\right)^2\left(\frac{k}{aH}\right)^{3-2\nu}. \tag{2.107}$$

and at the time of horizon exit we have

$$\mathcal{P}_\zeta = \left(\frac{H}{2\pi\dot{\phi}}\right)^2\Bigg|_{t(k)_{\rm exit}}. \tag{2.108}$$

We conclude this section mentioning that the curvature perturbation ζ introduced in (2.105) is a particular form of the gauge-invariant curvature perturbation on uniform-density hypersurfaces defined as

$$\zeta \equiv -\psi - H\frac{\delta\varrho}{\dot{\varrho}}, \tag{2.109}$$

where ψ is the scalar perturbation of the diagonal spatial component of the FRW metric. In fact, in equation (2.105) we considered the gauge choice $\psi = 0$, called uniform curvature gauge.

Chapter 3

Primordial Black Holes Formation

The detection of binary black hole mergers through gravitational waves by the LIGO-Virgo instrument [9] brought a significant increase of interest in models where Primordial Black Holes constitute a relevant fraction of dark matter. Indeed, the detected signal was generated by two merging black holes of mass approximately $30\mathrm{M}_{\odot}$, which is the mass range of interest for dark matter to comprise PBHs [10].

In this chapter we provide an introduction to the general relativistic formation of primordial black holes during radiation-dominated era and we summarize the main findings of Musco's work [11, 12, 13, 14].

The possibility that black holes could have formed in the early Universe was first raised by Bernard Carr and Stephen Hawking in Ref. [15]. PBHs could have been produced due to various mechanisms involving primordial density fluctuations generated during inflation (see section 2.4), or spontaneous formation due to a phase transition, for example from bubble collisions [16, 17, 18, 19], collapse of cosmic strings [20, 21, 22, 23, 24], necklaces [25, 26] or domain walls [27, 28].

We work on the first scenario, where very large primordial inhomogeneities, generated by quantum fluctuations in the inflaton field and stretched by the rapid inflationary expansion, eventually collapse gravitationally into a black hole. At zero order approximation, assuming that the primordial black hole forms immediately after the perturbation enters the horizon, denoting with M_{H} the horizon mass at horizon crossing, we find an estimation of the time of formation t_{f}

$$\begin{aligned} M_{\mathrm{PBH}} \sim M_{\mathrm{H}} &= \frac{4\pi}{3}\varrho_{\mathrm{H}} R_{\mathrm{H}}^3 \\ &= \frac{4\pi}{3}\frac{3H^2}{8\pi G}\left(\frac{c}{H}\right)^3 \\ &= \frac{c^3 t_{\mathrm{f}}}{G}, \end{aligned} \tag{3.1}$$

where we used the fact that $H \propto 1/(2t)$ during the radiation domination era. In equation (3.1), c is the speed of light, G is the gravitational constant, H is the Hubble constant, R_H is the Hubble radius and ϱ_H is the horizon energy density. We then obtain

$$t_{\mathrm{f}} = \frac{m_{\mathrm{PBH}} G}{c^3}. \tag{3.2}$$

This simple derivation gives us a rough glimpse on the mass range of PBHs, which is wide: while black holes resulting from astrophysical processes, such as the collapse of stars, cannot be

smaller than a certain mass (around $3M_\odot$), PBHs may be super-massive like stellar BHs (for example, those formed at 1 s would have a mass of order $10^5\ M_\odot$) but also as light as the Planck mass (those formed at Planck time 10^{-45} s would have mass 10^{-5} g).

3.1 Gradient Expansion Approximation

In the following section we review the main features of gradient expansion approximation [29, 30, 31], which are useful in the following discussion.

While cosmological perturbation theory expands the exact equations in powers of the perturbations keeping only terms of a finite order, the gradient expansion method is an expansion in the spatial gradient of these inhomogeneities. In particular, this procedure consists in multiplying each spatial gradient ∂_i at a fixed time by a fictitious parameter ϵ and in expanding the exact equations as a power series in ϵ. Finally, one keeps only the zero- and first-order terms and set $\epsilon = 1$ (see e.g., [29, 32, 33]).

We employ the metric in the standard $(3+1)$-decomposition of the ADM formalism [34]

$$\mathrm{d}s^2 = -N^2\mathrm{d}t^2 + \gamma_{ij}(\mathrm{d}x^i + \beta^i\mathrm{d}t)(\mathrm{d}x^j + \beta^j\mathrm{d}t), \tag{3.3}$$

where $\mathcal{N}$ is the lapse function, β^i the shift vector and γ_{ij} the 3-dimensional spatial metric. In general, this last term can be written as a product of two terms [29, 35]

$$\gamma_{ij} = a^2(t)\mathrm{e}^{2\zeta(t,x^i)}\widetilde{\gamma}_{ij}\ , \qquad \det[\widetilde{\gamma}_{ij}] = 1\ , \tag{3.4}$$

where $\zeta(t, x^i)$ is the curvature perturbation, here interpreted as the perturbation to the scale factor, and $\widetilde{\gamma}_{ij}$ is time independent. We assume that $\zeta(t, x^i)$ vanishes somewhere in the observable Universe such that $a(t)$ is the scale factor of that region and $\zeta(t, x^i)$ is a small perturbation throughout the observable Universe [29].

The gradient expansion approximation is useful to study non-linear perturbations whose characteristic scale L is much bigger than the horizon scale $1/(aH)$ [33]. In other words, every quantity can be assumed to be smooth on some sufficiently large scale with coordinate size k^{-1}. Focusing on the observable Universe, we can relate the perturbation length-scale L to the cosmological scale by $k = a(t)/L$, and conveniently identify [29, 33]

$$\epsilon \equiv \frac{k}{aH}. \tag{3.5}$$

The key assumption of this approach is that at a fixed time, in the limit $\epsilon \to 0$, which corresponds to $k \to 0$, the Universe becomes locally homogeneous and isotropic. Locally means that the region is smaller than the characteristic scale of the perturbation but larger than the horizon scale.

As a consequence of this assumption, there exist an appropriate set of coordinates which reduces the metric to the spatially flat FRW metric

$$ds^2 = -dt^2 + a^2(t)\delta_{ij}dx^i dx^j. \tag{3.6}$$

For the element of the metric in equation (3.3), this implies that $\beta = \mathcal{O}(\epsilon)$ whereas the time independent $\widetilde{\gamma}_{ij}$ can be removed by means of a local transformation of spatial coordinates. Therefore, we can rewrite equation (3.3) as

$$ds^2 = -N^2dt^2 + \beta^i dx^i dt + \gamma_{ij}dx^i dx^j. \tag{3.7}$$

Throughout the discussion, we assume to work with a perfect fluid, characterized by an equation of state of the form of equation (1.16)

$$p = w\varrho. \tag{3.8}$$

3.2 The curvature profile

Simulations of PBH formation have played a relevant role in understanding the relativistic aspects of critical collapse. Such simulation are performed working in the comoving gauge [35]. Here we give an overview of the main theoretical tools used to perform such simulations. First, we give a brief description of the Misner-Sharp equations, then we see how they provide the initial conditions for the numerical computations in terms of the curvature profile, $K(r)$. The physical properties of the curvature profile and its relation with the curvature perturbation will be discussed in the final part of the chapter.

Assuming spherical symmetry, we consider the metric [36]

$$\mathrm{d}s^2 = -A^2(t,\tilde{r})\mathrm{d}t^2 + B^2(t,\tilde{r})\mathrm{d}\tilde{r}^2 + R^2(t,\tilde{r})\mathrm{d}\Omega^2, \tag{3.9}$$

where r is the radial coordinate comoving with the fluid, A, B and R are positive definite functions of the time and radial coordinate. In the case of homogeneous and isotropic Universe, equation (3.9) reduces to the well-known FRW metric (1.2). Following the notation of Ref. [36], we introduce two basic differential operators

$$\begin{aligned} D_t &\equiv \frac{1}{A}\frac{\partial}{\partial t}, \\ D_{\tilde{r}} &\equiv \frac{1}{B}\frac{\partial}{\partial \tilde{r}}. \end{aligned} \tag{3.10}$$

that when applied to the function $R(t,\tilde{r})$ define two more quantities

$$\begin{aligned} U &\equiv D_t R = \frac{1}{A}\frac{\partial R}{\partial t}\ , \\ \Gamma &\equiv D_{\tilde{r}} R = \frac{1}{B}\frac{\partial R}{\partial \tilde{r}}\ , \end{aligned} \tag{3.11}$$

where U is the radial component of the four-velocity (in a non-comoving frame with radial coordinate R) and Γ is a generalization of the Lorentz factor. In the particular case of FRW metric (**??**) we get

$$\Gamma = \sqrt{1 - K\tilde{r}^2}, \tag{3.12}$$

therefore we can interpret Γ as a measure of the spatial curvature. Given the equation of state

describing the fluid (1.16), the set of Einstein's equations to solve is given by [12]

$$\begin{aligned}
D_t U &= -\left(\frac{\Gamma}{(\varrho_0+p)} D_{\tilde{r}} p + \frac{M}{R^2} + 4\pi R p\right), \\
D_t \varrho_0 &= -\frac{\varrho}{\Gamma R^2} D_{\tilde{r}}(R^2 U), \\
D_t \varrho &= \frac{\varrho + p}{\varrho_0} D_t \varrho_0, \\
D_t M &= -4\pi p U R^2, \\
D_{\tilde{r}} A &= -\frac{A}{\varrho + p} D_{\tilde{r}} p, \\
D_{\tilde{r}} M &= 4\pi R^2 \Gamma \varrho, \\
D_t \Gamma &= -\frac{U}{\varrho_0 + p} D_{\tilde{r}} p,
\end{aligned} \tag{3.13}$$

where ϱ_0 is the rest mass density. Furthermore, U and Γ can be related using the G_0^0 and G_0^1 components of the Einstein equations giving the so-called constraint equation

$$\Gamma^2 = 1 + U^2 - \frac{2M}{R}. \tag{3.14}$$

Since the numerical simulations are done assuming spherical symmetry, in the case where the spatial curvature K is position-dependent we conveniently introduce a generalized curvature profile $K(\tilde{r})$ in the FRW metric [12, 37]

$$\mathrm{d}s^2 = -\mathrm{d}t^2 + a^2 \left[\frac{\mathrm{d}\tilde{r}^2}{1 - K(\tilde{r})\tilde{r}^2} + \tilde{r}^2 \mathrm{d}\Omega^2\right], \tag{3.15}$$

therefore, using equation (3.12), the constraint equation (3.14) can be rewritten in term of the curvature profile as

$$-K(\tilde{r})\tilde{r}^2 = U^2 - \frac{2M}{R}. \tag{3.16}$$

Notice that in introducing $K(\tilde{r})$ in the FRW metric we loose homogeneity.

Following the gradient expansion approximation reviewed in section 3.1, we expand the metric component in equation (3.9) as

$$\begin{aligned}
A &= 1 + \epsilon^2 \tilde{A}, \\
B &= \frac{a(t)}{\sqrt{1 - K(\tilde{r})\tilde{r}^2}}(1 + \epsilon^2 \tilde{B}), \\
R &= a(t)\tilde{r}(1 + \epsilon^2 \tilde{R}),
\end{aligned} \tag{3.17}$$

knowing that for $\epsilon \ll 1$ it reduces to the metric in equation (3.15). We expand the hydrodynamical quantities as well as

$$\begin{aligned}
\varrho &= \bar{\varrho}(1 + \epsilon^2 \tilde{\varrho}), \\
U &= HR(1 + \epsilon^2 \tilde{U}), \\
M &= \bar{M}(1 + \epsilon^2 \tilde{M}),
\end{aligned} \tag{3.18}$$

where $\bar{\varrho}$ and $\bar{M} = 4\pi/3\bar{\varrho}R^3$ are respectively the background energy density and mass. We then replace these quantities in the equations (3.13) and in the constraint equation (3.14). Here, we

do not go into the details of the calculations, which are explicitly performed in Ref. [12], but we report the final expressions of relevance for our work.

From the gradient expansion approximation, the term of perturbation to the energy density in the first equation of (3.18) is given by

$$\tilde{\varrho} = \frac{3(1+w)}{5+3w}\left[K(\tilde{r}) + \frac{\tilde{r}}{3}K'(\tilde{r})\right]\tilde{r}_k^2\,, \tag{3.19}$$

where $\tilde{r}_k$ is the comoving lengthscale of the perturbation associated to the wavenumber k. Therefore, the energy density perturbation can be written as

$$\delta(\tilde{r}) \equiv \frac{\delta\varrho}{\bar{\varrho}} = \epsilon^2\tilde{\varrho} = \frac{3(1+w)}{5+3w}\left(\frac{1}{aH}\right)^2\left[K(\tilde{r}) + \frac{\tilde{r}}{3}K'(\tilde{r})\right]. \tag{3.20}$$

Notice that a singularity appears in equation (3.15) when $K(\tilde{r})\tilde{r}^2 = 1$. In order to avoid it, we should require that

$$1 - K(\tilde{r})\tilde{r}^2 > 0 \quad \Rightarrow \quad K(\tilde{r}) < \frac{1}{\tilde{r}^2}\,, \tag{3.21}$$

which corresponds to require that a perturbed spherical region of comoving radius $\tilde{r}$ should not be causally disconnected from the rest of the Universe.

We set the origin of our coordinate system at the peak and work with the isotropic metrics defined in equation (3.15). In Refs. [12, 35] the authors analysed the behaviour of "Gaussian-like" curvature profiles parametrised as

$$K_{\rm peak}(\tilde{r}) = \mathcal{A}_{\rm peak}\exp\left[-\frac{1}{2}\left(\frac{\tilde{r}}{\Delta}\right)^{2\alpha}\right], \tag{3.22}$$

where $\mathcal{A}_{\rm peak}$ is the peak amplitude, Δ is some typical scale of the perturbation and α is a parameter that describes the shape of the peak. In this case the density perturbation in equation (3.20) reads as

$$\delta_{\rm peak}(\tilde{r}) = \frac{3(1+w)}{5+3w}\frac{\mathcal{A}_{\rm peak}}{(aH)^2}\left[1 - \frac{\alpha}{3}\left(\frac{\tilde{r}}{\Delta}\right)^{2\alpha}\right]\mathrm{e}^{-\frac{1}{2}\left(\frac{\tilde{r}}{\Delta}\right)^{2\alpha}} \tag{3.23}$$

In figures 3.1 and 3.2 we show the curvature and density profile given by equations (3.22) and (3.23).

To give a complete overview, we derive the relation between the curvature profile $K(\tilde{r})$ and the primordial curvature perturbation ζ (see Section 2.4). However, in the following sections we employ only $K(\tilde{r})$.

We already saw that $K(\tilde{r})$ can be introduced in the FRW metric as in equation (3.15), whereas in the gradient expansion approximation the primordial curvature perturbation ζ can be interpreted as a perturbation to the scale factor $a(t)$

$$\mathrm{d}s^2 = -\mathrm{d}t^2 + a^2 e^{2\zeta(\hat{r})}\left[\mathrm{d}\hat{r}^2 + \hat{r}^2\mathrm{d}\Omega^2\right], \tag{3.24}$$

where the parametrisation of the radial comoving coordinate has now changed.

In order to find the relation between $K(\tilde{r})$ and $\zeta(\hat{r})$, we compare the angular and radial components

$$\begin{aligned} \hat{r}e^{\zeta(\hat{r})} &= \tilde{r}, \\ e^{\zeta(\hat{r})}d\hat{r} &= \frac{d\tilde{r}}{\sqrt{1 - K(\tilde{r})\tilde{r}^2}}, \end{aligned} \tag{3.25}$$

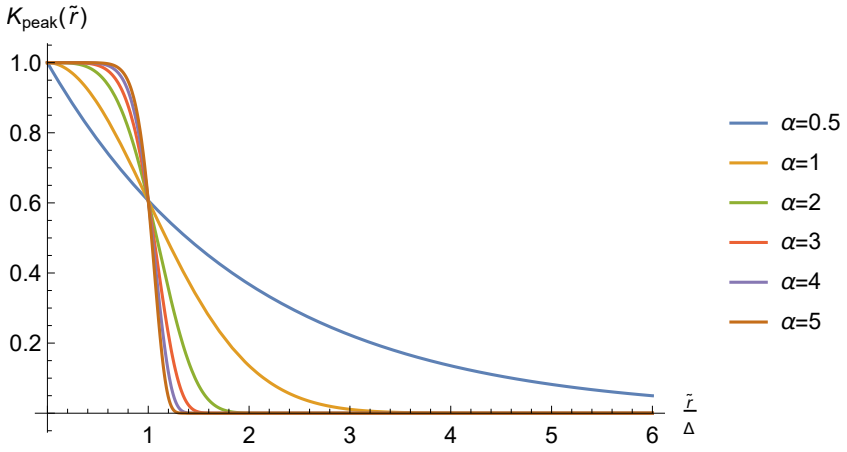

Figure 3.1: Curvature profiles for different shapes. Here we normalized all the amplitude to the unity.

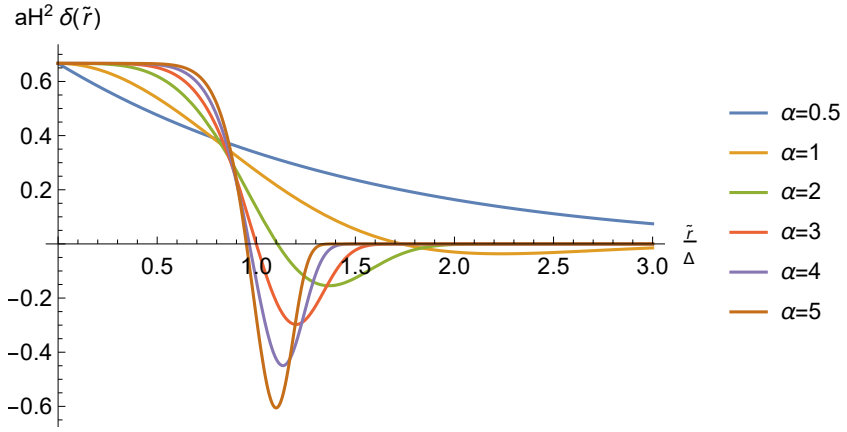

Figure 3.2: Density profiles for different shapes. Here we normalized all the amplitude to the unity.

and by differentiation of the first expression in equation (3.25), we obtain

$$\frac{d\tilde{r}}{d\hat{r}} = e^{\zeta(\hat{r})}[1 + \zeta'(\hat{r})\hat{r}], \tag{3.26}$$

where the prime $'$ indicates a derivative with respect to the radial coordinate. By replacing this equation into equation (3.25) we finally get

$$K(\tilde{r})\tilde{r}^2 = -\hat{r}\zeta'(\hat{r})[2 + \hat{r}\zeta'(\hat{r})]. \tag{3.27}$$

Given this relation, we can rewrite equation (3.20) in terms of $\zeta(\hat{r})$ as [35]

$$\delta(\hat{r}) = -\left(\frac{1}{aH}\right)^2 \frac{2(1+w)}{5+3w} e^{-2\zeta(\hat{r})}\left[\zeta''(\hat{r}) + \zeta'(\hat{r})\left(\frac{2}{\hat{r}} + \frac{\zeta(\hat{r})}{2}\right)\right]. \tag{3.28}$$

In the linear regime, where $\tilde{r} \simeq \hat{r}$, given the curvature profile $K(\tilde{r})$ of a spherically symmetric perturbation, equation (3.27) reduces to [35]

$$K(\hat{r}) \simeq -\frac{2}{r}\zeta'(r), \tag{3.29}$$

and the derivative of the curvature is given by

$$K'(\hat{r}) \simeq \frac{2}{r^2}\zeta'(r) - \frac{2}{r}\zeta''(r). \tag{3.30}$$

Finally, the density perturbation becomes

$$\delta(\hat{r}) \simeq -\left(\frac{1}{aH}\right)^2 \frac{2(1+w)}{5+3w}\left[\frac{2}{\hat{r}}\zeta'(\hat{r}) + \zeta''(\hat{r})\right] = -\left(\frac{1}{aH}\right)^2 \frac{2(1+w)}{5+3w}\nabla^2\zeta\ , \tag{3.31}$$

where

$$\nabla^2\zeta = \frac{1}{\hat{r}^2}\frac{d}{d\hat{r}}\left(\hat{r}^2\frac{d}{d\hat{r}}\zeta(\hat{r})\right). \tag{3.32}$$

is the Laplacian in spherical coordinates.

3.3 The threshold criterion

In this section we introduce new useful quantities to gain insight on the properties of the density perturbation profile. Let us define the background mass inside a cosmological horizon by $M_{\rm hor} = 4\pi\bar{\rho}R_{\rm hor}^3/3 = 4\pi M_P^2 c^3/H$. The mass excess inside some spherical region of radius r, that we call δ_I, is defined as

$$\frac{M(r,t) - M_{\rm hor}(t)}{M_{\rm hor}(t)} = \delta_I(r,t) = \frac{1}{V(t)}\int_\Omega d\Omega \int_0^r dr'(r')^2\delta(r',t) = \frac{3}{r^3}\int_0^r dr'(r')^2\delta(r',t), \tag{3.33}$$

where r' can be either $\tilde{r}$ or $\hat{r}$, since the above quantity must be gauge-independent.

Replacing the results obtained for the density perturbation (3.20), we have that

$$\begin{aligned}\delta_I(r) &= \left(\frac{1}{aH}\right)^2 \frac{3(1+w)}{5+3w}\frac{3}{r^3}\int_0^r \mathrm{d}r'^2 \frac{1}{3r'^2}\left[r'^3K(r')\right]' \\ &= \left(\frac{1}{aH}\right)^2 \frac{3(1+w)}{5+3w}\frac{1}{r^3}\left[r^3K(r)\right]_0^r \\ &= \left(\frac{1}{aH}\right)^2 \frac{3(1+w)}{5+3w}K(r).\end{aligned} \tag{3.34}$$

Notice that the function K slightly depends on time since every portion of the perturbation that is sub-horizon is evolving (see the discussion on the transfer function in section 4.2).

Before moving on, we explain the difference between compensated and non-compensated density profiles. The former are characterized by a region of overdensity of comoving radius r_0, defined as the zero of the density perturbation (3.23)

$$\delta(r_0) = 0 \quad \Rightarrow \quad K(r_0) + \frac{r_0}{3}K'(r_0) = 0, \tag{3.35}$$

surrounded by a region of underdensity. Non-compensated profile represent regions characterized by an overdensity that asymptotically goes to zero without encountering an underdensity region. In the case of compensated profile, it would be intuitive to integrate the mass excess in equation (3.34) up to r_0, namely assuming that all the mass in inside such radius. However, this interpretation does not consider whether the perturbation is all inside the horizon or just a part of it.

In presence of a spherical symmetry, as the perturbation collapses, we see the formation of an apparent horizon when the so-called compaction function [32]

$$\mathcal{C}(r,t) = 2\frac{M(r,t) - M_{\rm hor}(t)}{R(r,t)} \tag{3.36}$$

reaches its maximum and this maximum is above a certain threshold. In the equation above R is the areal radius. Because we are considering BHs, we have that the apparent horizon forms where $R = 2M_{\rm hor}$ [38] in natural units, therefore our compaction function corresponds exactly to our integrated profile δ_I defined in equation (3.34). The maximum of the compaction function, called $r_{\rm m}$, is defined by the differential equation

$$\mathcal{C}'(r_{\rm m}, t_{\rm m}) = \delta_I'(r_{\rm m}, t_{\rm m}) = 0 \quad \Longrightarrow \quad K(r_{\rm m}) + \frac{r_{\rm m}}{2}K'(r_{\rm m}) = 0, \tag{3.37}$$

where $t_{\rm m}$ is the horizon crossing time of the whole perturbation and it is defined implicitly by $a(t_{\rm m})H(t_{\rm m})r_{\rm m} = 1$. Therefore the correct criterion to establish the formation of a PBH is given by requiring that the integrated profile, calculated up to $r_{\rm m}$, is bigger than some critical value

$$\delta_I(r_{\rm m}, t_{\rm m}) > \delta_{I,{\rm c}}, \tag{3.38}$$

where perturbations that share the same $r_{\rm m}$ share also the same threshold.

In the case of the profiles reported in equation (3.22), $r_{\rm m}$ reads in terms of the typical scale as $r_{\rm m} = (2/\alpha)^{1/2\alpha}\,\Delta$, therefore we can rewrite equation (3.20) as

$$\delta_{\rm peak}(\tilde{r}, t) = \frac{3(1+w)}{5+3w}\frac{\mathcal{A}_{\rm peak}}{(aH)^2}\left[1 - \frac{2}{3}\left(\frac{\tilde{r}}{r_{\rm m}}\right)^{2\alpha}\right] e^{-\frac{1}{\alpha}\left(\frac{\tilde{r}}{r_{\rm m}}\right)^{2\alpha}} \tag{3.39}$$

and the threshold criterion reads as

$$\frac{3(1+w)}{5+3w}\frac{\mathcal{A}_{\rm peak}}{a_{\rm m}^2 H_{\rm m}^2}e^{-1/\alpha} = \delta_{\rm peak}(0, t_{\rm m})e^{-1/\alpha} > \delta_{I,{\rm c}}, \tag{3.40}$$

which can be approximately recast as

$$\delta_{\rm peak}(0, t_{\rm ab}) > \left(\frac{a_{\rm m}H_{\rm m}}{a_{\rm ab}H_{\rm ab}}\right)^2 e^{1/\alpha}\delta_{I,{\rm c}} = \left(\frac{a_{\rm ab}}{a_{\rm m}}\right)^2 e^{1/\alpha}\delta_{I,{\rm c}}, \tag{3.41}$$

where $a_{\rm ab} < a_{\rm m}$ is the scale factor when the PBHs abundance will be calculated.

Chapter 4

Peaks Theory

As we showed in chapter 2, the density inhomogeneities that seed the formation of structure in the Universe originated from quantum fluctuations arising during inflation. Cosmological density fluctuations are often assumed to be Gaussian random fields and the statistical properties of such fields are thoroughly addressed in Ref. [51]. Since the goal of Ref. [51] was to study Large Scale Structure (LSS) formation and abundance, the authors had in mind the matter-dominated era, where pressure effects are negligible. Nonetheless, the tools developed in Ref. [51] can be conveniently applied to the theory of PBHs formation under opportune assumptions.

In this chapter we first give the basic notions of Gaussian statistics and then derive the PBHs abundance in the framework of peaks theory.

4.1 The number density of extrema

In Ref. [51], the approach to the problem of non-linear evolution of structures focuses on the study of the local maxima of the initial density perturbations.The density perturbations is a Gaussian random field and in general in order to have a well-defined set of local maxima, the field must be smooth and differentiable.

An n-dimensional random field $F(\mathbf{r})$ is a set of random variables, one for each point $\mathbf{r}$ in the n-dimensional real space, defined by the set of finite-dimensional joint probability distribution functions

$$\text{prob}\left[F(\mathbf{r}_1), F(\mathbf{r}_2), \ldots, F(\mathbf{r}_j)\right] dF(\mathbf{r}_1) dF(\mathbf{r}_2) \ldots dF(\mathbf{r}_j). \tag{4.1}$$

A Gaussian random field is one for which the various j-point probability distributions defined above are multivariate Gaussians. A joint Gaussian probability distribution for random variables y_i reads as

$$P(y_1, \ldots, y_n) dy_1 \ldots dy_n = \frac{e^{-Q}}{[(2\pi)^n \det(M)]^{1/2}}, \quad Q = \sum_{ij} (\Delta y_i (M^{-1})_{ij} \Delta y_j)/2, \tag{4.2}$$

where only the mean values of the random variables $\langle y_i \rangle$ and their covariance matrix

$$M_{ij} = \langle \Delta y_i \Delta y_j \rangle, \quad \Delta y_i = y_i - \langle y_i \rangle, \tag{4.3}$$

are required to characterize the distribution.

For our purposes, we assume that initial density fluctuations are described by an isotropic, homogeneous Gaussian random fields with zero mean. We also assume that the field has been

previously smoothed out with some window function of radius R (for more details on the smoothing procedure see section 5.2). Such a field is completely specified by the power spectrum $P_R(k)$, or equivalently its Fourier transform, the correlation function $\xi_R(r)$. Since the Gaussian nature is retained throughout the linear regime, a complete statistical description of the local maxima can be extracted from the power spectrum.

The number density of points p that specify the maxima of the random field $F(\mathbf{r})$ is given by the point process equation

$$n_{pk}(\mathbf{r}) = \sum_p \delta^{(3)}(\mathbf{r} - \mathbf{r}_p). \tag{4.4}$$

One can restrict that class of points considering for example only those maxima above a certain threshold height. The number density (4.4) can be expressed in terms of the random field and its derivatives. Consider the Taylor expansion of $F(\mathbf{r})$ in the neighbourhood of a maximum point $\mathbf{r}_p$

$$\begin{aligned} F(\mathbf{r}) &= F(\mathbf{r}_p) + \partial_i F(\mathbf{r})|_{\mathbf{r}=\mathbf{r}_p}(r - r_p)_i + \frac{1}{2}\partial_i\partial_j F(\mathbf{r})|_{\mathbf{r}=\mathbf{r}_p}(r - r_p)_i(r - r_p)_j + \dots \\ &\approx F(\mathbf{r}_p) + \frac{1}{2}\theta_{ij}(r - r_p)_i(r - r_p)_j, \end{aligned} \tag{4.5}$$

where the first derivative $\eta_i(\mathbf{r}_p) = \partial_i F(\mathbf{r})|_{\mathbf{r}=\mathbf{r}_p} = 0$, the second derivative tensor $\theta_{ij} = \partial_i\partial_j F(\mathbf{r})|_{\mathbf{r}=\mathbf{r}_p}$ is negative definite given that $\mathbf{r}_p$ is a maximum, and

$$\eta_i(\mathbf{r}) \approx \sum_j \theta_{ij}(r - r_p)_j. \tag{4.6}$$

Since the θ-matrix is non-singular at the maximum point, we can invert equation (4.6)

$$\mathbf{r} - \mathbf{r}_p \approx \theta^{-1}(\mathbf{r}_p)\eta(\mathbf{r}), \tag{4.7}$$

and using the properties of the Dirac delta, we write

$$\delta^{(3)}(\mathbf{r} - \mathbf{r}_p) \approx |\mathrm{det}\theta(\mathbf{r}_p)|\delta^{(3)}(\eta(\mathbf{r})), \tag{4.8}$$

where the δ-function selects all the extremal points that are zeros of $\eta(\mathbf{r})$. Therefore, the number density of extrema (minima and maxima) in terms of field derivative can be expressed as

$$n_{ext}(\mathbf{r}) = |\mathrm{det}\theta(\mathbf{r}_p)|\delta^{(3)}(\eta(\mathbf{r})). \tag{4.9}$$

We find an identical expression for $n_{pk}(\mathbf{r})$ (4.4) with the additional condition of negativity on the three eigenvalues of θ_{ij} Moreover, if one selects only those maxima whose heights are in the range $[F_0, F_0 + dF]$ then a $\delta(F - F_0)dF$ should multiply equation (4.9). The ensemble average of $n_{ext}(\mathbf{r})$ is defined as

$$\langle n_{ext}(\mathbf{r})\rangle = \int \mathrm{d}F\mathrm{d}^6\theta\ |\mathrm{det}\theta(\mathbf{r}_p)|P(F, \eta = 0, \theta), \tag{4.10}$$

where P is the joint probability distribution defined in equation (4.2) From equation (4.10) we can derive the differential peak density that allows us to define the abundance of PBHs. The full computation of the integral can be found in Ref. [51], here we discuss the result. The distribution of fluctuations can be specified through the spectral moments

$$\sigma_j^2(\tau) = \int \frac{d^3k}{(2\pi)^3} P_R(k, \tau)k^{2j}, \tag{4.11}$$

where we notice that 0-th order spectral moment corresponds to the variance of the density fluctuation

$$\sigma_0^2(\tau) \equiv \sigma_R^2(\tau) = \xi_R(\mathbf{0}, \tau) = \int \frac{\mathrm{d}^3 k}{(2\pi)^3} P_R(k, \tau). \tag{4.12}$$

From the spectral moments, we infer the spectral parameters

$$\gamma(\tau) = \frac{\sigma_1^2(\tau)}{\sigma_2(\tau)\sigma_0(\tau)}, \qquad R_\star(\tau) = \sqrt{3}\frac{\sigma_1(\tau)}{\sigma_2(\tau)}. \tag{4.13}$$

Since in matter-domination, at linear order, the density field grows in a self-similar way, the spectral parameters above are time-independent and the comoving density of peaks does not depend on the time at which the density is measured, but this is not the case when pressure effects are important. The issue will be further discussed in section 4.2.

Finally, notice that the integral in equation (4.11) should be performed over all the momenta, since we are evaluating the statistical properties of the entire density field, so no sub- or super-horizon considerations apply here.

By denoting the peak height as $\delta_{\mathrm{peak}}(r = 0) = \delta_{\mathrm{peak},0}$ and introducing the parameter $\nu = \delta_{\mathrm{peak},0}/\sigma_0$, the authors of Ref. [51] found that the differential comoving peak density $dn_{\mathrm{peak}}^{\mathrm{com.}}/d\nu$ reads as

$$\frac{dn_{\mathrm{peak}}^{\mathrm{com.}}}{d\nu} = \frac{1}{(2\pi)^2 R_\star^3} e^{-\nu^2/2} G(\gamma, \gamma\nu), \tag{4.14}$$

where the function $G(\gamma, \gamma\nu)$, denoting $\omega = \gamma\nu$ can be approximated by

$$G(\gamma, \omega) \approx \frac{\omega^3 - 3\gamma^2\omega + [B(\gamma)\omega^2 + C_1(\gamma)]e^{-A(\gamma)\omega^2}}{1 + C_2(\gamma)e^{-C_3(\gamma)\omega}} \tag{4.15}$$

for $0.3 < \gamma < 0.7$ and for $-1 < \omega < +\infty$, keeping the error below the 1% level. The coefficients of the above equation reads as

$$\begin{gathered} A(\gamma) = \frac{5/2}{9 - 5\gamma^2}, \qquad B(\gamma) = \frac{432}{(10\pi)^{1/2}\left(9 - 5\gamma^2\right)^{5/2}}, \\ C_1(\gamma) = 1.84 + 1.13\left(1 - \gamma^2\right)^{5.72}, \qquad C_2(\gamma) = 8.91 + 1.27e^{6.51\gamma^2}, \qquad C_3(\gamma) = 2.58e^{1.05\gamma^2}. \end{gathered} \tag{4.16}$$

Not all the peaks will correspond to site where a more complex structure will form. Typically we have to introduce some threshold criterion, in our case we ask $\nu > \nu_c$ to have PBHs formation, where $\nu_c = e^{1/\alpha}\delta_{I,\mathrm{c}}/\sigma_0$ is given by equation (3.40).

4.2 PBHs Abundance from Peaks Theory

In this section, we derive the abundance of primordial black holes using the results of Ref. [51] paying attention to when they should be applyed. In fact, as stated in Ref. [52], the number of "high-enough" peaks that will form a PBH has to be calculated at some conformal initial time τ_{ab} when the perturbation is still super-horizon, in order for the results of Ref. [51] to be valid. For instance, the relative height ν of the peaks we are going to use in the following parts has been measure at τ_{ab} (this is important especially for measuring the variance σ_0).Moreover, we denote with τ_{m} the time when the perturbation crosses the horizon and becomes causally connected

for the first time and by defining as $\tau_{\rm f}$ the time of the PBH formation, we have from numerical simulations that $\tau_{\rm f}/\tau_{\rm m} = a_{\rm f}/a_{\rm m} = (t_{\rm f}/t_{\rm m})^{1/2} \simeq 3$. The differential physical peak density reads as

$$\frac{dn^{\rm phys.}_{\rm peak}(\nu,\tau_{\rm f})}{d\nu} = a^{-3}(\tau_{\rm f})\frac{dn^{\rm com.}_{\rm peak}(\nu,\tau_{\rm ab})}{d\nu}. \tag{4.17}$$

We define the relative energy density of PBHs with respect to radiation energy density at formation as

$$\beta_{\rm f} = \beta(\tau_{\rm f}) = \frac{\rho_{\rm PBH}(\tau_{\rm f})}{\rho_{\rm r}(\tau_{\rm f})} \simeq \beta(\tau_{\rm eq})\frac{a_{\rm f}}{a_{\rm eq}} = f_{\rm PBH}\frac{a_{\rm f}}{a_{\rm eq}}, \tag{4.18}$$

where $\tau_{\rm eq}$ is the time of matter-radiation equality, $f_{\rm PBH} = \rho_{\rm PBH}/\rho_{\rm dm}$ is the fraction of dark matter made by PBHs and we have used the fact that at equality $\rho_{\rm dm} = \rho_{\rm r}$. Notice that our definition of $\beta_{\rm f}$ is slightly different from the one used in Ref. [52], where they define it as a ratio between the PBHs energy density and the baryon energy density. Using the result from peaks theory we have that

$$\beta_{\rm f} = \frac{1}{\rho_{\rm r}(\tau_{\rm f})}\int_{\nu_c}^{\infty} d\nu \frac{d\rho^{\rm phys.}_{\rm PBH}(\nu,\tau_{\rm f})}{d\nu}, \tag{4.19}$$

where

$$\frac{d\rho^{\rm phys.}_{\rm PBH}(\nu,\tau_{\rm f})}{d\nu} = M_{\rm PBH}(\nu,\tau_{\rm m})\frac{dn^{\rm phys.}_{\rm peak}(\nu,\tau_{\rm f})}{d\nu} \tag{4.20}$$

and the PBH mass has been calculated at horizon crossing and reads as [53, 54, 55, 13]

$$M_{\rm PBH}(\nu,\tau_{\rm m}) = \mathcal{K}_{\rm peak}M_{\rm hor}(\tau_{\rm m})(\delta_{\rm peak,0} - \delta_{\rm peak,0,c})^{\gamma} = \mathcal{K}_{\rm peak}M_{\rm hor}(\tau_{\rm m})\sigma_0^{\gamma}(\tau_{\rm ab})(\nu-\nu_{\rm c})^{\gamma}, \tag{4.21}$$

where $M_{\rm hor}(\tau_{\rm m}) = 4\pi M_P^2 c^3/H(\tau_{\rm m})$ is the mass inside the horizon at horizon crossing, $\gamma \simeq 0.36$ is a critical exponent that depends on the equation of state in the formation era [56] and $\mathcal{K}_{\rm peak}$ is a numerical coefficient that depends on the specific density profile and on how we "measure" the perturbation, namely through the height of the peak (as in our case) or through the integrated profile. Notice that the two possibilities described differ only by a multiplicative factor $e^{-1/\alpha}$, as can be seen in equation (3.40), that can be easily reabsorbed in the $\mathcal{K}$ coefficient. The result in the above equation holds under the condition $M_{\rm PBH} \lesssim M_{\rm hor}$.

Replacing equations (4.20) and (4.21) in the definition of $\beta_{\rm f}$ given in equation (4.19), we have

$$\begin{aligned}\beta_{\rm f} &= \frac{\mathcal{K}_{\rm peak}M_{\rm hor}(\tau_{\rm m})\sigma_0^{\gamma}(\tau_{\rm ab})}{\rho_{\rm r}(\tau_{\rm f})}\int_{\nu_c}^{\infty} d\nu(\nu-\nu_{\rm c})^{\gamma}\frac{dn^{\rm phys.}_{\rm peak}(\nu,\tau_{\rm f})}{d\nu} \\ &= \frac{\mathcal{K}_{\rm peak}M_{\rm hor}(\tau_{\rm m})\sigma_0^{\gamma}(\tau_{\rm ab})}{(2\pi)^2\rho_{\rm r}(\tau_{\rm f})a(\tau_{\rm f})^3R_\star^3}\int_{\nu_c}^{\infty} d\nu(\nu-\nu_{\rm c})^{\gamma}e^{-\nu^2/2}G(\gamma,\gamma\nu),\end{aligned} \tag{4.22}$$

where in the second line we used equation (4.14). The radiation energy density at the formation time is given by $\varrho_{\rm r}(\tau_{\rm f}) \simeq 3\mathcal{H}^2/8\pi G$, where $\mathcal{H}$ is the Hubble parameter in terms of the conformal time.

Finally, using the saddle-point approximation in the limit of very high peaks, the authors of Ref. [52] find that

$$\beta_{\rm f} = \mathcal{C}\nu_{\rm c}e^{-\nu_c^2/2} \tag{4.23}$$

where for the sake of clarity we denoted the terms given by the integration that do not depend on ν as

$$\mathcal{C} = \sqrt{\frac{2}{\pi}}\mathcal{K}_{\rm peak}M_{\rm hor}(\tau_{\rm m})\sigma_0^{\gamma}(\tau_{\rm ab})k_\star^3\gamma^{\gamma+1/2}, \tag{4.24}$$

where $k_\star = \gamma(\tau)/R_\star$ defined in equation (4.13).

4.3 Profile Shape

In this section we discuss the average profile shape we expect the peak to have, following the discussion in [51]. We define $\nu(r) = \delta_R(r)/\sigma_0$ and

$$\psi(r_{ij}) = \langle \nu(r_i)\nu(r_j)\rangle = \frac{\langle \delta_R(r_i)\delta_R(r_j)\rangle}{\sigma_0^2} = \frac{\xi_R(r_{ij})}{\sigma_0^2}, \tag{4.25}$$

where the smoothing radius has been chosen smaller than the typical scale of the peak.

Let us suppose that at $r = 0$ there is a peak of height ν, then the mean value of the density at distance r (and so the average shape around the peak), after averaging over all possible curvatures (i.e., second derivatives) and orientations (i.e., ellipticity and prolateness/oblateness), reads as [51]

$$\frac{\bar{\delta}_{\rm peak}(r)}{\sigma_0} = \nu\psi(r) - \frac{\theta(\gamma,\gamma\nu)}{\gamma(1-\gamma^2)}\left[\gamma^2\psi(r) + \frac{\nabla^2\psi(r)}{3}\right], \tag{4.26}$$

where

$$\theta(\gamma,\omega) = \frac{3(1-\gamma^2) + (1.216 - 0.9\gamma^4)e^{-2\gamma/\omega^2}}{\left[3(1-\gamma^2) + 0.45 + \frac{\omega^2}{4}\right]^{1/2} + \frac{\omega}{2}} \tag{4.27}$$

is accurate for $\gamma \in [0.4, 0.7]$ and $\omega \in [1, 3]$. On the other hand, the average density structure around a point with the same height ν as the peak (but which is not a peak) reads as [57, 58]

$$\frac{\bar{\delta}_{\text{no peak}}(r)}{\sigma_0} = \nu\psi(r), \tag{4.28}$$

where equations (4.26) and (4.28) coincide in the limit of high ν. Of course not all peaks share the same shape, therefore we can associate to the mean profiles introduced in equations (4.26) and (4.28) a variance of shapes $\sigma^2_{\rm shape}(r)$ which is slightly different in the two cases. For high peaks the variance is small, however at large enough distance it will be as large as the amplitude of the peak in that point. When this happens, at some radial distance that we call $r_{\rm dec}$, the fluctuation loses its coherence.

Since we consider high peaks (or alternatively, rare events) we can neglect the correction given by $\theta(\gamma, \gamma\nu)$ and work directly with

$$\xi_R(r) = \sigma_0^2 \frac{\bar{\delta}_{\rm peak}(r)}{\bar{\delta}_{\rm peak}(0)}, \tag{4.29}$$

which is valid up to the decoherence radius $r_{\rm dec}$ (see Ref. [58]). For greater distances the density fluctuations are basically uncorrelated, but we do not have any estimate of the two point correlation function $\tilde{\xi}_R(r) \equiv \xi_R(r > r_{\rm dec})$. Equivalently, one can also work with the Fourier transform of equation (4.29), which reads as[1]

$$\begin{aligned} P_R(k) &= \int d^3r \xi_R(r) e^{-i\mathbf{k}\cdot\mathbf{r}} \\ &= 4\pi\left[\sigma_0^2 \int_0^{r_{\rm dec}} dr\ r^2 \frac{\sin(kr)}{kr}\frac{\bar{\delta}_{\rm peak}(r)}{\bar{\delta}_{\rm peak}(0)} + \int_{r_{\rm dec}}^{\infty} dr\ r^2 \frac{\sin(kr)}{kr}\tilde{\xi}_R(r)\right]. \end{aligned} \tag{4.30}$$

[1] Recall that

$$\int d\Omega e^{-i\mathbf{k}\cdot\mathbf{r}} = 4\pi\frac{\sin(kr)}{kr}.$$

Notice however that as long as we work with modes $k \gtrsim k_{\rm dec} = 1/r_{\rm dec}$ the second integral should be negligible with respect to the first one because of the suppression given by the $\sin(x)/x$ factor. Therefore we limit our analysis to those modes.

Chapter 5

Primordial Power Spectrum

In this chapter we compute the primordial curvature perturbation power spectrum profile for different shapes of the density perturbations provided by the relativistic numerical simulations reviewed in chapter 3 and we show that the formation of PBHs in real space leads to a pronounced bump in the power spectrum $\mathcal{P}_\zeta$ of the curvature perturbation. The goal is to use the constraints on PBHs abundance deriving from experimental observations to put an upper bound limit on the amplitudes of the primordial curvature perturbations that could collapse into PBHs.

5.1 The Transfer Function

So far we have applied the theory developed in Ref. [51] (see chapter 4) to derive fundamental properties of PBHs, such as the abundance in section 4.2 and the profile shape of the density perturbations in section 4.3. However, we emphasize that the results of Ref. [51] are valid for some initial field or for some linearly evolved field, whereas the formation of primordial black holes requires very large perturbations that might evolve in a non-linear way. Therefore, it is crucial to decide when to apply the results of Ref. [51] in the context of PBHs formation.

According to the inflationary paradigm, density perturbation in the radiation field δ are generated by curvature perturbation ζ at horizon re-entry via Poisson equation (see e.g., Ref. [6])

$$\delta(\mathbf{x}) = \frac{2}{3}\frac{1}{a^2H^2}\nabla^2\Phi(\mathbf{x}), \tag{5.1}$$

where Φ is the Bardeen potential (also gravitational potential in Poisson gauge) at super-horizon scales. Here, for adiabatic perturbation and neglecting non-linear corrections, Φ and the primordial curvature perturbation ζ are related by

$$\Phi(\mathbf{x}) = -\frac{3(1+w)}{5+3w}\zeta(\mathbf{x}), \tag{5.2}$$

therefore we have that equation (5.1) becomes

$$\delta(\mathbf{x}) = \frac{2}{3}\frac{1}{a^2H^2}\nabla^2\Phi(\mathbf{x}) = -\frac{2(1+w)}{5+3w}\frac{1}{a^2H^2}\nabla^2\zeta(\mathbf{x}), \tag{5.3}$$

as we found in equation (3.31) at linear level. In Fourier space, this equation reads as

$$\delta(\mathbf{k}) = -\frac{2(1+w)}{5+3w}\frac{k^2}{a^2H^2}\zeta(\mathbf{k}). \tag{5.4}$$

Equation (5.2) tells us that the Bardeen potential is constant at super-horizon scales, however Φ evolves differently at sub-horizon scale depending on whether the perturbations re-enter the horizon during the radiation-dominated epoch or the matter-dominated epoch [6].

In the case of LSS formation (matter-dominated Universe), the pressure effects are negligible and the linear equation for the gravitational potential Φ reads as [6]

$$\Phi'' + 3\mathcal{H}\Phi' = 0, \tag{5.5}$$

therefore the total evolution is going be determined by a growth factor $D(\tau)$ (solution of the above equation) and by a transfer function $\mathcal{T}(k)$ that describes the evolution of perturbations through the epochs of horizon crossing and radiation/matter transition. Notice that in this context all modes k grow in the same way since there is no pressure or any mode coupling. This also means that the statistical properties of the density field, i.e. the spectral moments, simply evolves with the growth factor.

The same does not happen in radiation-domination, where we have pressure effects and the gravitational potential evolves as

$$\Phi'' + 4\mathcal{H}\Phi' + c_s^2 k^2 \Phi = 0, \tag{5.6}$$

where $c_s^2 = 1/3$ is the sound speed of the relativistic fluid. In this case the statistical properties of the density field change in time in a non-trivial way and we can only write a "global" transfer function (see e.g., Ref. [59] and Refs. therein)

$$\mathcal{T}(k,\tau) = 3\frac{\sin(k\tau/\sqrt{3}) - (k\tau/\sqrt{3})\cos(k\tau/\sqrt{3})}{(k\tau/\sqrt{3})^3}, \tag{5.7}$$

Nevertheless we may apply the results of Ref. [51] on super-horizon scales, where there are no pressure effects, and we take account of the evolution of sub-horizon modes including the transfer function (5.7) in equation (5.4) (see e.g., Ref. [60, 61, 59])

$$\delta(\mathbf{k}) = -\frac{2(1+w)}{5+3w}\frac{k^2}{a^2H^2}\mathcal{T}(k,\tau)\zeta(\mathbf{k}). \tag{5.8}$$

5.2 The Window Function

In chapter 4 the results were derived assuming that all the density pertubation $\delta(\mathbf{x})$ had already been smoothed on some scale R. In fact, as already emphasized in Ref. [51], since random fields are not differentiable, a window function is absolutely necessary to define properties of random fields as peaks or troughs. In this section, we introduce the concept of window function and we discuss why it should be treated with special care in the framework of PBHs formation.

On the other hand, the window function is just a mathematical artefact we introduce to treat analytically random fields. It is of primary importance to check that such procedure does not bias the final result, or in case it does, to estimate the magnitude of such bias.

Going back to the equation (5.3) written in section 5.1, we point out that the real Gaussian random field is ζ, however, since the Laplacian is a linear operator, the radiation field is Gaussian too. Nevertheless the statistics of the radiation field will deviate from the Gaussian one once higher order corrections are taken into account. In fact, the smoothing procedure is a highly nonlinear and nonlocal procedure, hence statistics of smoothed fields can deviate from Gaussian statistics, even if fields themselves are Gaussian.

The smoothed density field is given by the convolution with a window function W_R of characteristic radius R

$$\delta_R(\mathbf{x}) = \int d^3y W_R(|\mathbf{x}-\mathbf{y}|)\delta(\mathbf{y}). \tag{5.9}$$

Typical choices of window functions are the Top-hat window function

$$W_R^{\text{Top Hat}}(|\mathbf{x}-\mathbf{y}|) = \left(\frac{4\pi R^3}{3}\right)^{-1} \Theta\left(1-\frac{|\mathbf{x}-\mathbf{y}|}{R}\right) \tag{5.10}$$

or the Gaussian window function

$$W_R^{\text{Gaussian}}(|\mathbf{x}-\mathbf{y}|) = \left(2\pi R^2\right)^{-3/2} e^{-|\mathbf{x}-\mathbf{y}|^2/(2R^2)}, \tag{5.11}$$

but other choices are also possible.

In principle there could be some ambiguity on which field has to be smoothed out, if the radiation field δ or the curvature field ζ. However, at linear order, the two possibilities are equivalent, in fact if we apply the smoothing procedure to equation (5.3) we obtain

$$\begin{aligned}
\delta_R(\mathbf{x}) &= \int d^3y W_R(|\mathbf{x}-\mathbf{y}|)\delta(\mathbf{y}) \\
&= \frac{2(1+w)}{5+3w}\frac{1}{a^2H^2}\int d^3y W_R(|\mathbf{x}-\mathbf{y}|)\nabla^2_{\mathbf{y}}\zeta(\mathbf{y}) \\
&= \frac{2(1+w)}{5+3w}\frac{1}{a^2H^2}\int d^3y \left\{\zeta(\mathbf{y})\nabla^2_{\mathbf{y}}W_R(|\mathbf{x}-\mathbf{y}|)\right. \\
&\qquad \left. +\nabla_{\mathbf{y}}\cdot[W_R(|\mathbf{x}-\mathbf{y}|)\nabla_{\mathbf{y}}\zeta(\mathbf{y}) - \zeta(\mathbf{y})\nabla_{\mathbf{y}}W_R(|\mathbf{x}-\mathbf{y}|)]\right\},
\end{aligned} \tag{5.12}$$

where we have used the relation $\psi\nabla^2\phi = \phi\nabla^2\psi + \nabla\cdot(\psi\nabla\phi - \phi\nabla\psi)$ between two generic scalar fields $\psi(\mathbf{x})$ and $\phi(\mathbf{x})$. The second term in the integrand is a surface contribution and vanishes using divergence theorem, under the fairly general assumption that W_R and its derivative vanish at large scales. Furthermore, at least for the two window functions in equations (5.10) and (5.11), we have that $\nabla^2_{\mathbf{y}}W_R = \nabla^2_{\mathbf{x}}W_R$, therefore the above equation reads as

$$\delta_R(\mathbf{x}) = \frac{2(1+w)}{5+3w}\frac{1}{a^2H^2}\int d^3y \zeta(\mathbf{y})\nabla^2_{\mathbf{x}}W_R(|\mathbf{x}-\mathbf{y}|) = \frac{2(1+w)}{5+3w}\frac{1}{a^2H^2}\nabla^2_{\mathbf{x}}\zeta_R(\mathbf{x}), \tag{5.13}$$

which is the smoothed version of equation (5.3), as we expected. This proves the equivalence between smoothing out the density or the curvature field at linear level.

Since the smoothing procedure involves a convolution, we know from the convolution theorem in Fourier analysis that in Fourier space this is a simple multiplication of Fourier transforms, therefore

$$\zeta_R(\mathbf{k}) = W_R(k)\zeta(\mathbf{k}), \tag{5.14}$$

where $W_R(k)$ is the Fourier transform of the window function. In particular, in Fourier space the two window functions introduced in equations (5.10) and (5.11) read as

$$W_R^{\text{Top Hat}}(k) = 3\frac{\sin(kR)-(kR)\cos(kR)}{k^3R^3}, \qquad W_R^{\text{Gaussian}}(k) = e^{-\frac{1}{2}k^2R^2}. \tag{5.15}$$

In the end, the complete relation between smoothed density field and curvature perturbation reads as

$$\delta_R(\mathbf{k},\tau) = -\frac{2(1+w)}{5+3w}\frac{k^2}{a^2H^2}\mathcal{T}(k,\tau)W_R(k)\zeta(\mathbf{k}). \tag{5.16}$$

We now address the issue of the determination of which modes k play a physical role in the collapse, which in turn will determine the appropriate value of the smoothing radius. In fact, the smoothing procedure may have non-trivial effects related to the choice of the smoothing radius; we refer the interested reader to Refs. [59, 62] for effects on PBHs constraints and to Ref. [63] for a similar effects applied to dark matter halos.

So far in the literature the smoothing radius has been chosen to be equal to the radius of the horizon when the perturbation starts to collapse, namely $R \sim \mathcal{O}(r_m)$. On one hand this choice is motivated by the fact that the mass of a PBH is proportional to the mass inside the horizon when the collapse starts, so it seems natural to put a Top Hat window function to separate the collapsing region from the non-collapsing one. On the other hand we should always keep in mind that the window function is a mathematical artefact. When choosing the smoothing radius to be of the same size of the perturbation, we are implicitly introducing significant uncertainties. This is why some authors find that the constraint on PBHs are highly dependent on the choice of the window function [59].

In our case, the typical scale of a perturbation is identified with r_m in real space or $k_m = r_m^{-1}$ in Fourier space (see equation (3.37)). Then, as in the large scale structure (LSS) framework, we want to smooth out modes $k \gg k_m$ or, equivalently, small scale fluctuations $r \ll r_m$, to define the characteristics of the peaks. Notice that the specifics details on how these modes are smoothed out cannot influence the dynamics of the perturbation on scales $\mathcal{O}(r_m)$, where the collapse is happening; moreover this procedure is naturally implemented every time that the spacetime is discretized, as in numerical simulations. Furthermore, in the radiation-dominated era, every fluctuation on small scales, i.e. deeply sub-horizon, that is not close enough to the critical threshold will be naturally washed out because of radiation pressure, as we see in section 5.1. This is a crucial difference from what happens in the LSS framework, since in that context the gravitational collapse happens in matter domination, where there are no pressure effect during the first stages of the collapse[1]. The natural conclusion seems to be that the smoothing radius should be chosen as $R \ll r_m$, in order to not spoil artificially the shape of the peak, which ultimately will determine the shape of the power spectrum. We emphasize that the of smoothing radius is not "universal", in the sense that different profiles that collapse at different times require different smoothing radii. However, the requirement $R \ll r_m$ should be true for all of this radii. The underneath assumption in this reasoning is that PBHs form only at one scale (i.e., we have no "black-hole-in-black-hole" problem, similar to the "cloud-in-cloud" issue in LSS).

In the study of PBHs collapse high k modes are not the only troublesome modes, in fact we should worry also of low k ones. We know that modes $k \ll k_m$ appear as a constant background during the first stages of the collapse, therefore they should not play any role in determining whether PBHs form or not. Also in this case we should smooth out these modes introducing a second smoothing radius such that $R' \gg r_m$, and the details of such smoothing should not affect the collapse. In conclusion, one cannot rigidly apply the LSS framework to the study of PBHs collapse exactly because of this problem of the small k modes.

To be consistent with what explained before we have to smooth out scales much smaller and much bigger than the typical scale of the perturbation, so in principle we need two smoothing radii. As pointed out in section 4.3, for fluctuations described by high peaks there exists a decohorence radius $r_{\rm dec}$ where the fluctuation loses coherence. Since we do not go into the details of the physics beyond the decoherence radius described by the second term on the right-hand-side of equation (4.30), we do not introduce a second smoothing radius for small k modes.

[1] On the other hand pressure effects appear and are important during the latest phases, e.g., during virialization.

As we discussed in Section 2.5 , the statistical properties of random fields, in this case of the curvature perturbation, are given by the n-point correlators $\langle\zeta(\mathbf{k}_1)\cdots\zeta(\mathbf{k}_n)\rangle$, in particular we are interested in the two-point function in Fourier space specified by primordial curvature power spectrum P_ζ as in equation (2.86). In this particular case we have

$$\langle\zeta(\mathbf{k}_1)\zeta(\mathbf{k}_2)\rangle = (2\pi)^3\delta^{(3)}\left(\mathbf{k}_1+\mathbf{k}_2\right)P_\zeta(k_1), \tag{5.17}$$

At cosmological scales ($k \lesssim 1$ Mpc^{-1}) we have measured that the power spectrum is almost scale invariant and reads as

$$P_\zeta(k) = \frac{2\pi^2 A_s}{k^3}\left(\frac{k}{k_{\text{pivot}}}\right)^{n_s-1}, \tag{5.18}$$

where A_s is the scalar perturbations amplitude, n_s is the scalar tilt and k_{pivot} is the pivot scale[2].

Finally, the power spectrum of the smoothed radiation density field reads as

$$P_R(k) = W_R^2(k)P_\delta(k) = \left[\frac{2(1+w)}{5+3w}\frac{k^2}{a^2H^2}\right]^2 W_R^2(k)\mathcal{T}^2(k,\tau)P_\zeta(k), \tag{5.19}$$

where P_δ is the power spectrum of the unsmoothed radiation density field. This key equation allows us to connect PBHs to the primordial curvature power spectrum coming from inflation. Moreover, this power spectrum is in turn the Fourier transform of the two-point correlation functions in real space, in particular we have for the smoothed radiation field that

$$\xi_R(|\mathbf{x}_1-\mathbf{x}_2|) = \langle\delta_R(\mathbf{x}_1)\delta_R(\mathbf{x}_2)\rangle = \int\frac{\mathrm{d}^3k}{(2\pi)^3}P_R(k)e^{i\mathbf{k}\cdot(\mathbf{x}_1-\mathbf{x}_2)}. \tag{5.20}$$

5.3 Constraints on the Curvature Power Spectrum

Given the assumptions and the results provided in the previous sections, in this section we first compute $P_\zeta(k)$ for two different shape of the density perturbation and then use the constraints on PHBs abundance to limit the amplitude of the resulting power spectra.

First of all, we have to establish the magnitude of r_{dec}. For compensated profiles, as those reported in equation (3.22), it always exists some radius r_0 where the density perturbation profile becomes zero. From equation (3.35) we have that r_0 is defined as

$$r_0 = \left(\frac{3}{2}\right)^{\frac{1}{2\alpha}} r_m. \tag{5.21}$$

At this distance the profile has already lost its coherence (see section 4.3) since the density perturbation structure at this point is far from that of the peak, therefore r_0 is a good candidate to identify with the decoherence radius. However, we point out that this is just an approximation, in fact is very likely that the decoherence happens before, for example near r_m. Nevertheless we choose $r_{\text{dec}} = r_0$ and we study only modes $k \gtrsim k_0 = r_0^{-1}$.

Secondly, we expect the characteristic scale of formation in real space, r_{m}, to have a correspondent scale in the Fourier space, i.e. k_{m} such that $r_{\text{m}} = 1/k_{\text{m}}$. Since r_{m} implicitly defines the time when the whole perturbation enters the horizon (see section 3.3), assuming that the perturbation collapses immediately after horizon crossing k_m is the cosmological scale

[2] According to the latest Planck collaboration results [64], we have $A_s = 2.105\cdot10^{-9}$ and $n_s = 0.9665$ measured at $k_{\text{pivot}} = 0.05$ Mpc^{-1}.

where the bump in the power spectrum forms and it is related to the mass $M_{\rm PBH}$ defined in equation (3.1). In particular, knowing that during radiation domination $aH \propto a^{-1}$ and expansion at constant entropy gives $\varrho_H \propto a^{-4}$ (see e.g. [3], notice that a more complete computation take into account also the contribution of the number of relativistic degrees of freedom g_*), then the horizon mass evolves as

$$M_{\rm H} \simeq M_{\rm H,eq} \left(\frac{k_{\rm eq}}{k}\right)^2, \tag{5.22}$$

where we used the fact that at horizon crossing $k = aH$. With "eq" we denote parameters at matter-radiation equality, which are given by $k_{\rm eq} \simeq 0.01$ Mpc^{-1} and $M_{\rm H,eq} \simeq 1.3 \times 10^{45} \omega_m^{-2}$ g, with $\omega_m = 0.14$ [64]. Going into solar masses units, we have that [59]

$$M_{\rm PBH} \sim M_\odot \left(\frac{k_{\rm m}}{4.2 \times 10^6 {\rm Mpc}^{-1}}\right)^{-2}, \tag{5.23}$$

which gives an estimation of $k_{\rm m}$.

5.3.1 Primordial curvature power spectra

We compute the power spectra for primordial black holes of four different masses in units of solar masses: $M_{\rm PBH} = 10^{-2}, 1, 10^2, 10^4$, from which using equation (3.2) we derive the time of formation $t_{\rm f}$. Combining equations (5.19), (4.30) and the density perturbation profile in (3.39), we have that

$$\begin{aligned} W_R^2(k)\mathcal{T}^2(k,\tau)P_\zeta(k) &\approx \left(\frac{aH}{k}\right)^4 \left(\frac{5+3w}{2(1+w)}\right)^2 4\pi\sigma_0^2 \int_0^{r_0} dr\ r^2 \frac{\sin(kr)}{kr} \left[1 - \frac{2}{3}\left(\frac{r}{r_m}\right)^{2\alpha}\right] e^{-(r/r_m)^{2\alpha}/\alpha} \\ &= \left(\frac{aH}{k}\right)^4 \left(\frac{5+3w}{2(1+w)}\right)^2 4\pi\sigma_0^2 r_m^3 \int_0^{(3/2)^{1/2\alpha}} dx\ x^2 \frac{\sin(kr_m x)}{kr_m x} \left[1 - \frac{2}{3}x^{2\alpha}\right] e^{-x^{2\alpha}/\alpha} \\ &= \left(\frac{aH}{k}\right)^4 \left(\frac{5+3w}{2(1+w)}\right)^2 4\pi\sigma_0^2 r_m^3 \times \mathcal{I}(kr_m, \alpha), \end{aligned} \tag{5.24}$$

where in the second passage we used the coordinate transformation $x = r/r_m$ the integral $\mathcal{I}$ depends only on the combination kr_m, once α, i.e. the shape of the profile, is fixed.

Moreover, using the definition of dimensionless power spectrum $\mathcal{P}_\zeta(k)$ in equation (2.89), equation (5.24) reads as

$$\mathcal{P}_\zeta(k) \approx \frac{2}{\pi k} \left(\frac{5+3w}{2(1+w)}\right)^2 \frac{\mathcal{A}_{\rm peak}^2 r_m^3}{\log \beta_{\rm f}^{-2}} \times \frac{\mathcal{I}(kr_m, \alpha)}{W_R^2(k)\mathcal{T}^2(k,\tau)}. \tag{5.25}$$

We have to estimate σ_0^2. As seen in section 4.2, the PBH abundance $\beta_{\rm f}$ is given by equation (4.23), we can be roughly approximated as

$$\beta_{\rm f} \sim \exp\left(-\frac{\nu_c^2}{2}\right), \tag{5.26}$$

therefore we have that

$$\sigma_0^2(\tau) \approx \frac{\mathcal{A}_{\rm peak}^2}{\log \beta_{\rm f}^{-2}} (aH)^{-4}. \tag{5.27}$$

In our results, we use a Top-hat window function as in equation (5.10) with a smoothing radius given by $R = r_{\rm m}/10$, the transfer function is that of equation (5.7). The last ingredient we need is the abundance that can be evaluated using equation (4.18). For our results we assume that primordial black holes provide all the dark matter, therefore we put $f_{\rm PBH} = 1$. In this case,we expect the abundance to change with the value of the mass since PBHs with a smaller mass need a smaller initial abundance to form. Again, from Ref. [64] we have that the scale factor at matter-radiation equality time is given by $a_{\rm eq} = 1/(1 + z_{\rm eq}) = 1/3402$. The scale factor at formation $a_{\rm f}$ is calculated using the condition $k_{\rm m} = a_{\rm f} H_{\rm f}$.

We consider here a couple of cases, corresponding to the profiles $\alpha = 1/2$ and $\alpha = 1$. In this case, from numerical simulations we have that

$$\mathcal{A}_{\rm peak} r_m^2 = \begin{cases} 5.175 & \alpha = 1/2, \\ 2.025 & \alpha = 1. \end{cases} \tag{5.28}$$

In table 5.1 we report the resulting values.

Mass ($M_\odot$)	$t_{\rm f}$ (s)	$k_{\rm m}$ (Mpc^{-1})	$r_{\rm m}$ (Mpc)	$\beta_{\rm f}$
10^{-2}	4.9×10^{-8}	4.2×10^{7}	2.4×10^{-8}	1.4×10^{-10}
1	4.9×10^{-6}	4.2×10^{6}	2.4×10^{-7}	1.4×10^{-9}
10^{2}	4.9×10^{-4}	4.2×10^{5}	2.4×10^{-6}	1.4×10^{-8}
10^{4}	4.9×10^{-2}	4.2×10^{4}	2.4×10^{-5}	1.4×10^{-7}

Table 5.1: Values of the parameters used in the computation of the power spectra.

In figures 5.1 and 5.2 we show the behaviour of power spectrum $\mathcal{P}_\zeta(k)$ for small and large scales. For both figures, in the case of large scales, i.e. small k-modes ($k < 10$ Mpc^{-1}), we have the nearly scale invariant power spectrum (see equation (5.18)), whereas for small scale, namely for k-modes greater than each k_m, we have the power spectrum of the peaks described by equation (5.25). The intermediate scales are determined by processes of early clustering of PBHs, whose treatment is beyond the scope of this work. We refer the interested reader to Refs. [65, 66, 67, 68, 69], where a complete presentation of the topic is given. Here, we give a guess of the behaviour of the power spectrum based on previous literature, where the formation of PBHs leads to a spike or a bump in the primordial power spectrum in the neighbourhood of $k_{\rm m}$. Finally, we notice that all the power spectra on small scales present oscillations which are more pronounced when $\alpha = 1$. We are not sure why we observe such behaviour, but a probable reason could lie in the computation of the density perturbation profiles in section 3.2. Here, in order to be consistent with the numerical results we computed the density perturbation profiles as a function of the curvature profile $K_{\rm peak}$, instead of the curvature perturbation ζ, which is the true perturbation generated during inflation.

As predicted, both figures show an increase of the amplitude of the power spectra going from smaller masses to bigger ones. This increment is subtle because of the logarithmic dependence of the amplitude on the intial abundance $\beta_{\rm f}$, as seen in equation (5.25). However, the power spectra computed from the density perturbation with $\alpha = 1/2$ generally show larger amplitudes than the profiles with $\alpha = 1$. This is because the density profile with $\alpha = 1/2$ is more peaked than the one with $\alpha = 1$, as it can be seen in figure 3.2.

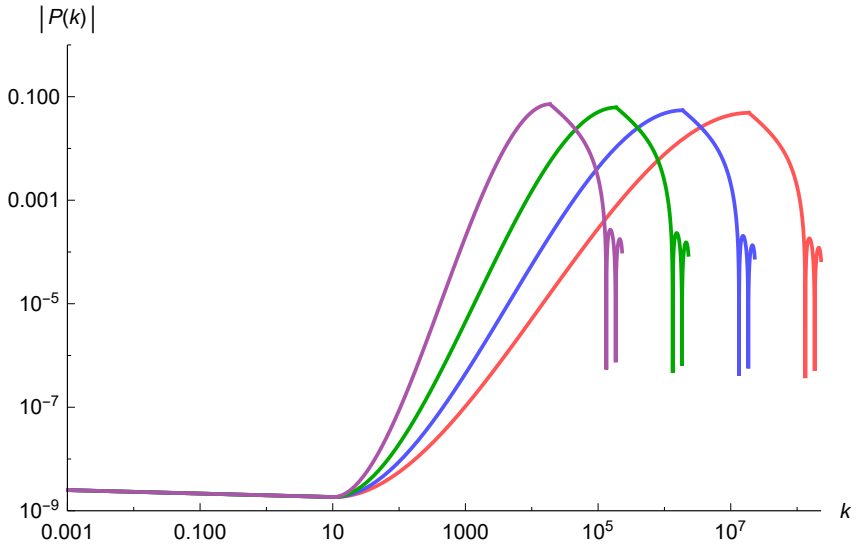

Figure 5.1: Power spectra for $\alpha = 1$. From the right to the left we have $10^{-2}M_\odot$ (red), $1M_\odot$ (blue), $10^2M_\odot$ (green) and $10^4M_\odot$ (purple).

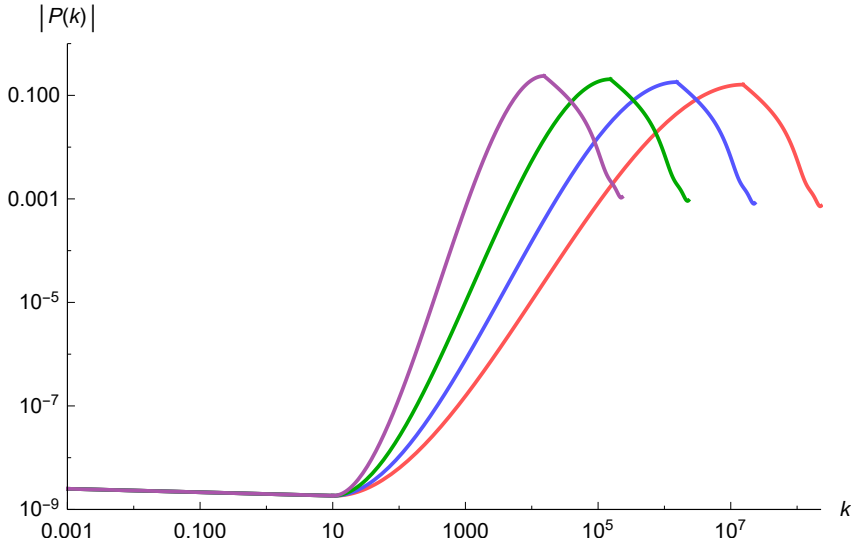

Figure 5.2: Power spectra for $\alpha = 1/2$. From the right to the left we have $10^{-2}M_\odot$ (red), $1M_\odot$ (blue), $10^2M_\odot$ (green) and $10^4M_\odot$ (purple).

5.3.2 Constraints on the amplitude of the power spectrum

In this subsection, we use the constraints on the fraction of PBHs in dark matter $f_{\rm PBH}$ shown in figure 5.3 to put an upper limit on the amplitude of the power spectrum $\mathcal{P}_\zeta(k_{\rm m})$ [46]. These constraints are derived by investigating the observational effects given by gravitational lensing caused by PBHs, and gravitational interactions of PBHs with astrophysical objects, such as neutron stars and wide binaries.

In the previous subsection, we limited our analysis to the case of four different PBHs masses and $f_{\rm PBH} = 1$. Here, instead, we expand the study to masses in the range $[10^{-16}, 10^4]$ $M_\odot$, and

Mass range ($M_\odot$)	Source
$10^{-16}, 10^{-15}$	Femtolensing
10^{-14} and $[10^{-12}, 10^{-9}]$	Neutron Star Disruption
10^{-13}	HSC (microlensing)
$10^{-8}, 10^{-7}$	Kepler (microlensing)
$[10^{-6}, 10^{-4}]$ and $[1, 10^2]$	EROS (microlensing)
$[10^{-3}, 10^{-1}]$ and 10^4	Caustic (microlensing)
10^3	Wide Binaries Disruption

Table 5.2: Source of the constraint based on the mass of the PBH, extracted from 5.3.

we compare the amplitude of the power spectrum in equation (5.25) for each mass in the case where $f_{\text{PBH}} = 1$ with the amplitudes given by the values of f_{PBH} extracted from figure 5.3. The extracted constraints show that the in general PBHs constitute only a fraction of dark matter, as $f_{\text{PBH}} < 1$. In table 5.2 we list the origin of the constraints for each mass value.

Figures 5.4 and 5.5 show the amplitude of the power spectrum for respectively $\alpha = 1$ and $\alpha = 1/2$; we notice that while there is a difference between the constrained and the unconstrained amplitudes, such difference is suppressed because, as we already discussed, the contribution of the abundance in the power spectrum is logarithmic. Finally, as previously observed, while both graphs show the same behaviour, the amplitudes in the case of $\alpha = 1/2$ are larger than the ones in the case of $\alpha = 1$.

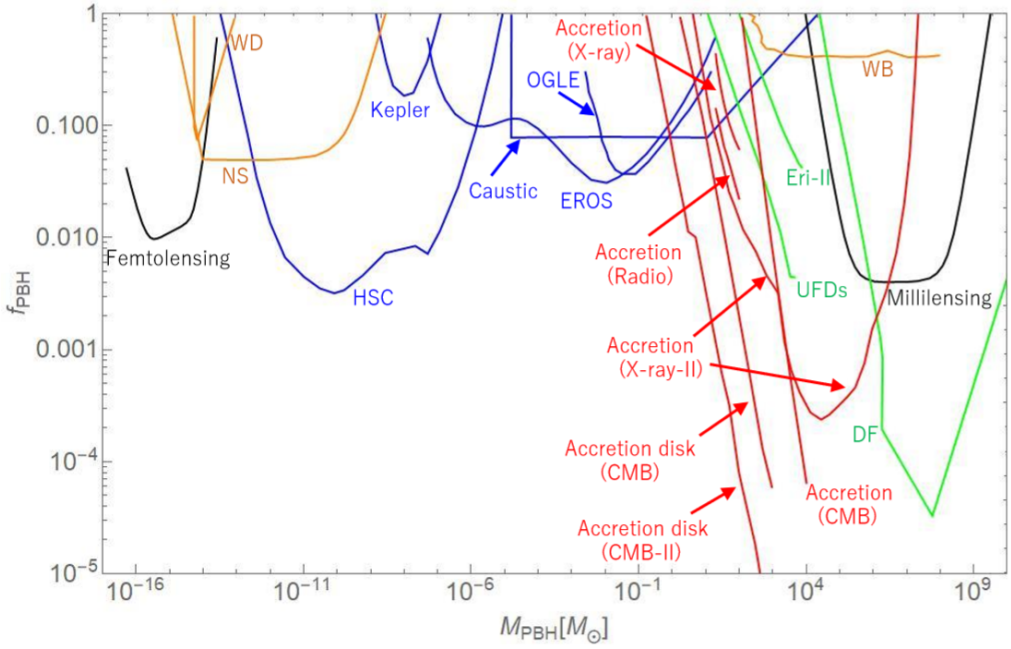

Figure 5.3: Upper limit on f_{PBH} for various PBH masses [46].

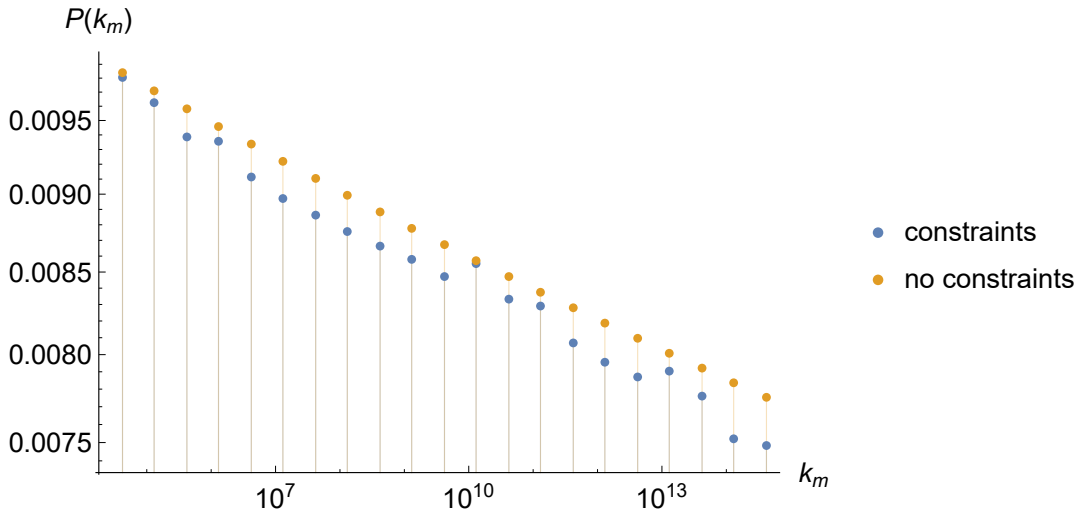

Figure 5.4: Amplitudes of the power spectra at $k = k_{\mathrm{m}}$ for $\alpha = 1$.

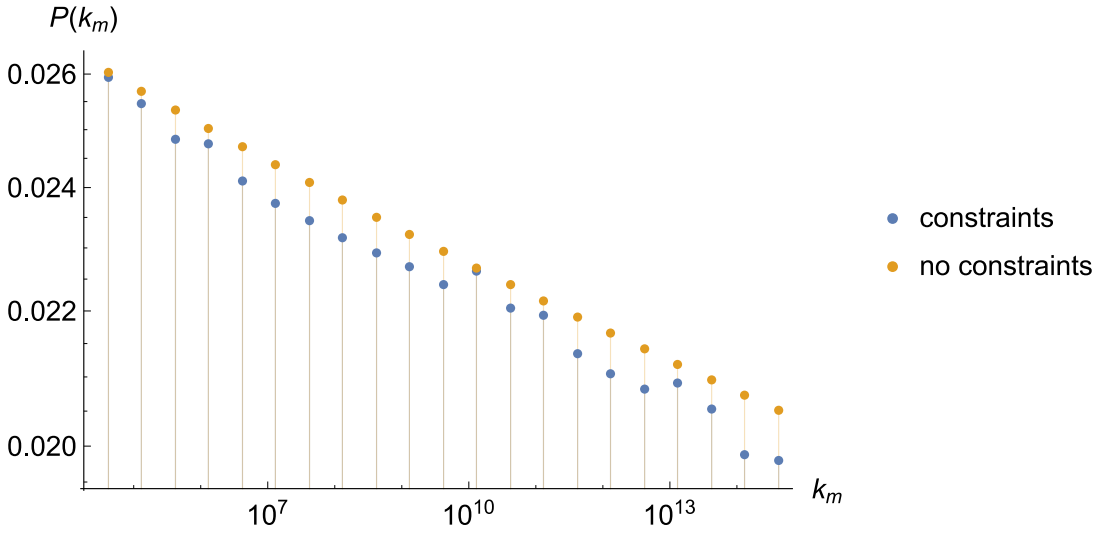

Figure 5.5: Amplitudes of the power spectra at $k = k_{\mathrm{m}}$ for $\alpha = 1/2$

.

Chapter 6

Conclusions

This work aimed to constrain the amplitude of the power spectrum associated to the formation of primordial black holes by means of current observational constraints on the PBHs abundance. First, we computed the primordial curvature power spectrum including the details of PBHs formation in real space obtained from numerical simulations. This methodology has the advantage that it provides the initial density perturbation profile that generates PBHs starting from different shapes of the curvature profile.

We applied the main results of peaks theory to the primordial black hole scenario in order to derive the abundance and to predict the profile shape of the peaks that lead to PBHs formation. In doing so, we paid attention to the assumptions needed for peaks theory to be valid.

We discussed some aspects of the window function that are essentials in our case. First of all, we had to understand if the window function had to be applied to curvature perturbation or density perturbation field. We proved that, at least at the linear level and in the case of the top-hat window function and gaussian window function, it is equivalent to smooth out the density or the curvature field. Moreover, we paid particular case in choosing the smoothing radius, which it is crucial if one wants to avoid large uncertainties in the computation of the power spectrum related to the choice of the window function. Indeed, if we take the smoothing radius to be of the same order of the characteristic scale of the primordial black hole formation, as done in previous literature, the peak associated to such formation is biased.

The power spectra resulting from our procedure show, as predicted, a bump at the characteristic scale of PBHs formation. We then computed the amplitude of such peaks in the case where PBHs constitute all of dark matter, and we compared the results with amplitudes obtained employing observational constraints on PBHs abundance in dark matter. In this way, we find the maximum amplitude of the bump in the power spectrum necessary to generate PBHs of a certain mass.

The results of this work can be employed to discern the various inflationary models that generate the perturbations need to PBHs formation, such as the running-mass model (see e.g. Refs. [43, 44]) and the inflection-point model (see e.g. Refs. [45, 50, 39]). Indeed, we can compare the enhancement in the primordial power spectrum predicted by these models with the amplitudes we computed starting from gravitational collapse in real space.

Bibliography

[1] T. Bringmann, P. Scott, and Y. Akrami, "Improved constraints on the primordial power spectrum at small scales from ultracompact minihalos", Phys. Rev. D **85** (Jun, 2012) 125027, arXiv:1110.2484.

[2] A. R. Liddle and D. H. Lyth, Cosmological inflation and large scale structure. 2000.

[3] E. W. Kolb and M. S. Turner, The Early Universe, vol. 69. 1990.

[4] D. H. Lyth and A. R. Liddle, The primordial density perturbation: Cosmology, inflation and the origin of structure. 2009.

[5] P. Coles and F. Lucchin, Cosmology: The Origin and evolution of cosmic structure. 1995.

[6] S. Dodelson, Modern cosmology. Academic Press, San Diego, CA, 2003. https://cds.cern.ch/record/1282338.

[7] D. Baumann, "Inflation", in Physics of the large and the small, TASI 09, proceedings of the Theoretical Advanced Study Institute in Elementary Particle Physics, Boulder, Colorado, USA, 1-26 June 2009, pp. 523–686. 2011. arXiv:0907.5424.

[8] N. Bartolo, E. Komatsu, S. Matarrese, and A. Riotto, "Non-Gaussianity from inflation: theory and observations", Physics Reports **402** no. 3, (2004) 103 – 266.

[9] The **LIGO Scientific Collaboration and Virgo Collaboration**, B. P. e. a. Abbott, "Observation of Gravitational Waves from a Binary Black Hole Merger", Phys. Rev. Lett. **116** (Feb, 2016) 061102.

[10] S. Bird, I. Cholis, J. B. Muñoz, Y. Ali-Haïmoud, M. Kamionkowski, E. D. Kovetz, A. Raccanelli, and A. G. Riess, "Did LIGO detect dark matter?", Phys. Rev. Lett. **116** no. 20, (2016) 201301, arXiv:1603.00464.

[11] I. Musco, J. C. Miller, and L. Rezzolla, "Computations of primordial black hole formation", Classical and Quantum Gravity **22** (2005) 1405–1424, arXiv:gr-qc/0412063.

[12] A. G. Polnarev and I. Musco, "Curvature profiles as initial conditions for primordial black hole formation", Classical and Quantum Gravity **24** (2007) 1405–1432, arXiv:gr-qc/0605122.

[13] I. Musco, J. C. Miller, and A. G. Polnarev, "Primordial black hole formation in the radiative era: investigation of the critical nature of the collapse", Classical and Quantum Gravity **26** no. 23, (2009) 235001, arXiv:0811.1452.

[14] I. Musco and J. C. Miller, "Primordial black hole formation in the early universe: critical behaviour and self-similarity", Classical and Quantum Gravity **30** (2013) 145009, arXiv:1201.2379.

[15] B. J. Carr and S. W. Hawking, "Black Holes in the Early Universe", Monthly Notices of the Royal Astronomical Society **168** no. 2, (Aug, 1974) 399–415. https://doi.org/10.1093/mnras/168.2.399.

[16] S. W. Hawking, I. G. Moss, and J. M. Stewart, "Bubble Collisions in the Very Early Universe", Phys. Rev. **D26** (1982) 2681.

[17] M. Crawford and D. N. Schramm, "Spontaneous generation of density perturbations in the early Universe", Nat **298** (Aug, 1982) 538–540.

[18] I. G. Moss, "Singularity formation from colliding bubbles", Phys. Rev. **D50** (1994) 676–681.

[19] R. V. Konoplich, S. G. Rubin, A. S. Sakharov, and M. Y. Khlopov, "Formation of black holes in first-order phase transitions in the Universe", Astronomy Letters **24** (Jul, 1998) 413–417.

[20] S. W. Hawking, "Black holes from cosmic strings", Physics Letters B **231** (Nov, 1989) 237–239.

[21] J. Garriga and M. Sakellariadou, "Effects of friction on cosmic strings", Phys. Rev. **D48** (1993) 2502–2515, arXiv:hep-th/9303024.

[22] R. R. Caldwell and P. Casper, "Formation of black holes from collapsed cosmic string loops", Phys. Rev. **D53** (1996) 3002–3010, arXiv:gr-qc/9509012.

[23] R. N. Hansen, M. Christensen, and A. L. Larsen, "Cosmic string loops collapsing to black holes", Int. J. Mod. Phys. **A15** (2000) 4433–4446, arXiv:gr-qc/9902048.

[24] J. H. MacGibbon, R. H. Brandenberger, and U. F. Wichoski, "Limits on black hole formation from cosmic string loops", Phys. Rev. **D57** (1998) 2158–2165, arXiv:astro-ph/9707146.

[25] T. Matsuda, "Primordial black holes from cosmic necklaces", JHEP **04** (2006) 017, arXiv:hep-ph/0509062.

[26] M. Lake, S. Thomas, and J. Ward, "String Necklaces and Primordial Black Holes from Type IIB Strings", JHEP **12** (2009) 033, arXiv:0906.3695.

[27] S. G. Rubin, M. Yu. Khlopov, and A. S. Sakharov, "Primordial black holes from nonequilibrium second order phase transition", Grav. Cosmol. **6** (2000) 51–58, arXiv:hep-ph/0005271.

[28] R. R. Caldwell, A. Chamblin, and G. W. Gibbons, "Pair creation of black holes by domain walls", Phys. Rev. **D53** (1996) 7103–7114, arXiv:hep-th/9602126.

[29] D. H. Lyth, K. A. Malik, and M. Sasaki, "A General proof of the conservation of the curvature perturbation", JCAP **0505** (2005) 004, arXiv:astro-ph/0411220.

[30] Y. Tanaka and M. Sasaki, "Gradient expansion approach to nonlinear superhorizon perturbations", Prog. Theor. Phys. **117** (2007) 633–654, arXiv:gr-qc/0612191.

[31] Y. Tanaka and M. Sasaki, "Gradient expansion approach to nonlinear superhorizon perturbations. II. A Single scalar field", Prog. Theor. Phys. **118** (2007) 455–473, arXiv:0706.0678.

[32] M. Shibata and M. Sasaki, "Black hole formation in the Friedmann universe: Formulation and computation in numerical relativity", Phys. Rev. **D60** (1999) 084002, arXiv:gr-qc/9905064.

[33] N. Deruelle and D. Langlois, "Long wavelength iteration of Einstein's equations near a spacetime singularity", Phys. Rev. D **52** (Aug, 1995) 2007–2019.

[34] R. Arnowitt, S. Deser, and C. W. Misner, "Republication of: The dynamics of general relativity", General Relativity and Gravitation **40** no. 9, (Sep, 2008) 1997–2027.

[35] I. Musco, "The threshold for primordial black holes: dependence on the shape of the cosmological perturbations", arXiv:1809.02127.

[36] C. W. Misner and D. H. Sharp, "Relativistic Equations for Adiabatic, Spherically Symmetric Gravitational Collapse", Physical Review **136** no. 2B, (Oct, 1964) B571–B576.

[37] A. G. Polnarev, T. Nakama, and J. Yokoyama, "Self-consistent initial conditions for primordial black hole formation", JCAP **1209** (2012) 027, arXiv:1204.6601.

[38] A. Helou, I. Musco, and J. C. Miller, "Causal nature and dynamics of trapping horizons in black hole collapse", Classical and Quantum Gravity **34** no. 13, (2017) 135012, arXiv:1601.05109.

[39] H. Motohashi and W. Hu, "Primordial Black Holes and Slow-Roll Violation", Phys. Rev. **D96** no. 6, (2017) 063503, arXiv:1706.06784.

[40] E. D. Stewart, "Flattening the inflaton's potential with quantum corrections", Phys. Lett. **B391** (1997) 34–38, arXiv:hep-ph/9606241 [hep-ph].

[41] E. D. Stewart, "Flattening the inflaton's potential with quantum corrections. 2.", Phys. Rev. **D56** (1997) 2019–2023, arXiv:hep-ph/9703232 [hep-ph].

[42] D. H. Lyth and A. Riotto, "Particle physics models of inflation and the cosmological density perturbation", Phys. Rept. **314** (1999) 1–146, arXiv:hep-ph/9807278.

[43] S. M. Leach, I. J. Grivell, and A. R. Liddle, "Black hole constraints on the running mass inflation model", Phys. Rev. **D62** (2000) 043516, arXiv:astro-ph/0004296.

[44] M. Drees and E. Erfani, "Running-Mass Inflation Model and Primordial Black Holes", JCAP **1104** (2011) 005, arXiv:1102.2340.

[45] J. Garcia-Bellido and E. Ruiz Morales, "Primordial black holes from single field models of inflation", Phys. Dark Univ. **18** (2017) 47–54, arXiv:1702.03901.

[46] M. Sasaki, T. Suyama, T. Tanaka, and S. Yokoyama, "Primordial black holes—perspectives in gravitational wave astronomy", Classical and Quantum Gravity **35** no. 6, (Feb, 2018) 063001. https://doi.org/10.1088/1361-6382/aaa7b4.

[47] J. Garcia-Bellido, D. G. Figueroa, and J. Rubio, "Preheating in the Standard Model with the Higgs-Inflaton coupled to gravity", Phys. Rev. **D79** (2009) 063531, arXiv:0812.4624.

[48] F. L. Bezrukov and M. Shaposhnikov, "The Standard Model Higgs boson as the inflaton", Phys. Lett. **B659** (2008) 703–706, arXiv:0710.3755.

[49] J. M. Ezquiaga, J. Garcia-Bellido, and E. Ruiz Morales, "Primordial Black Hole production in Critical Higgs Inflation", Phys. Lett. **B776** (2018) 345–349, arXiv:1705.04861.

[50] C. Germani and T. Prokopec, "On primordial black holes from an inflection point", Physical Review D (Sep, 2017) .

[51] J. M. Bardeen, J. R. Bond, N. Kaiser, and A. S. Szalay, "The statistics of peaks of Gaussian random fields", The Astrophysical Journal **304** (May, 1986) 15.

[52] C. Germani and I. Musco, "The abundance of primordial black holes depends on the shape of the inflationary power spectrum", arXiv:1805.04087.

[53] M. W. Choptuik, "Universality and scaling in gravitational collapse of a massless scalar field", Phys. Rev. Lett. **70** (Jan, 1993) 9–12.

[54] J. C. Niemeyer and K. Jedamzik, "Near-Critical Gravitational Collapse and the Initial Mass Function of Primordial Black Holes", Phys. Rev. Lett. **80** (Jun, 1998) 5481–5484, arXiv:astro-ph/9709072.

[55] J. C. Niemeyer and K. Jedamzik, "Dynamics of primordial black hole formation", Phys. Rev. D **59** (May, 1999) 124013, arXiv:astro-ph/9901292.

[56] D. W. Neilsen and M. W. Choptuik, "Critical phenomena in perfect fluids", Classical and Quantum Gravity **17** no. 4, (2000) 761, arXiv:gr-qc/9812053.

[57] S. O. Rice, "Mathematical Analysis of Random Noise", Bell System Technical Journal **23** no. 3, (1944) 282–332.

[58] A. Dekel, "Imprints of the Damping of Adiabatic Perturbations", A&A **101** (Aug, 1981) 79.

[59] K. Ando, K. Inomata, and M. Kawasaki, "Primordial black holes and uncertainties in the choice of the window function", Phys. Rev. D **97** (May, 2018) 103528, arXiv:1802.06393.

[60] D. Blais, T. Bringmann, C. Kiefer, and D. Polarski, "Accurate results for primordial black holes from spectra with a distinguished scale", Phys. Rev. D **67** (Jan, 2003) 024024, arXiv:astro-ph/0206262.

[61] A. S. Josan, A. M. Green, and K. A. Malik, "Generalized constraints on the curvature perturbation from primordial black holes", Phys. Rev. D **79** (May, 2009) 103520, arXiv:0903.3184.

[62] C. Byrnes, I. Musco, and S. Young, "PBHs and Window Function", in prep. (2018) .

[63] L. Verde, R. Jimenez, F. Simpson, L. Alvarez-Gaume, A. Heavens, and S. Matarrese, "The bias of weighted dark matter haloes from peak theory", Monthly Notices of the Royal Astronomical Society **443** no. 1, (2014) 122–137, arXiv:1404.2241.

[64] The **Planck Collaboration**, N. Aghanim et al., "Planck 2018 results. VI. Cosmological parameters", arXiv:1807.06209.

[65] J. R. Chisholm, "Clustering of primordial black holes: Basic results", Phys. Rev. D **73** (Apr, 2006) 083504, arXiv:astro-ph/0509141.

[66] J. R. Chisholm, "Clustering of primordial black holes. II. Evolution of bound systems", Phys. Rev. D **84** (Dec, 2011) 124031, arXiv:1110.4402.

[67] Y. Ali-Haïmoud, "Correlation function of high-threshold peaks and application to the initial (non)clustering of primordial black holes", arXiv:1805.05912.

[68] V. Desjacques and A. Riotto, "The Spatial Clustering of Primordial Black Holes", arXiv:1806.10414.

[69] G. Ballesteros, P. D. Serpico, and M. Taoso, "On the merger rate of primordial black holes: effects of nearest neighbours distribution and clustering", arXiv:1807.02084.